Earth-Science Reviews 208 (2020) 103255

Contents lists available at ScienceDirect

Earth-Science Reviews

journal homepage: www.elsevier.com/locate/earscirev

Rejuvenation of ancient micro-continents during accretionary orogenesis: Insights from the Yili Block and adjacent regions of the SW Central Asian Orogenic Belt

He Huang[a,*], Tao Wang[a,b,*], Ying Tong[a], Qie Qin[a], Xuxuan Ma[a], Jiyuan Yin[a]

[a] Key Laboratory of Deep-Earth Dynamics of the Ministry of Natural Resources, Institute of Geology, Chinese Academy of Geological Sciences, Beijing 100037, China
[b] Beijing SHRIMP Center, Institute of Geology, Chinese Academy of Geological Sciences, Beijing 100037, China

ARTICLE INFO

Keywords:
Hf isotopic mapping
SW CAOB
Yili Block
Continental growth
Retreating subduction

ABSTRACT

In the Central Asian Orogenic Belt (CAOB), whether substantial juvenile additions associated with accretionary orogenesis are preserved is still a pending issue. The Yili Block (YB) is a micro-continent in the Western Tianshan, SW CAOB. Voluminous felsic rocks constitute two major belts stretching in the southern and northern margins of the YB. We synthetically compile up-to-date zircon U-Pb geochronological, elemental, and Nd-Hf isotopic data for felsic rocks from the YB and adjacent tectonic domains. Spatially, Hf-Nd isotopic mapping unveils an inboard-younging trend in Hf model age of the YB, which indicates relative ancient basement rocks in its northern and southern edges and the most juvenile crust beneath its centre. Temporally, the compiled zircon Hf isotopic dataset suggests alternating continental reworking and growth in the YB and adjacent regions during Paleozoic times. In combination with other evidence, we speculate that the Paleozoic continental evolution in the Yili Block and adjacent regions were associated with episodic advancing and retreating subduction of branches of the Paleo-Asian Ocean (i.e., North Tianshan Ocean in the north and South Tianshan Ocean in the south) and the following orogenic collage. Continental arc-type felsic rocks yield two major populations of ~460 to ~395 Ma and ~375 to ~310 Ma, respectively, implying two epochs of subduction events punctuated by a magmatic lull. In the first-stage subduction, tectonic switch from advancing to retreating subduction took place around ~450 Ma in the northern YB and ~420 Ma in the southern YB. The second-stage subduction was characterized by a period of trench advance (~ 375 to ~350 Ma in the northern YB and ~370 to ~350 Ma in the southern YB) at the initiation and the following Early Carboniferous trench retreat (~350 to ~310 Ma in the northern YB, and ~350 to ~322 Ma in the southern YB) associated with the development of back-arc basins. The final assembly of the Western Tianshan orogenic collage plausibly occurred during the Late Carboniferous. In the south, a "hard" collision followed the closure of the South Tianshan Ocean. On the contrary, the northern margin of the YB was likely collided "softly" with an immature/nascent island arc.

The current study highlights a crucial link between supra-subduction extension triggered by trench retreat (slab rollback) and the continental growth of the Yili Block and adjacent regions. On a larger scale, such a long-term "rejuvenation" process, which was characterized by the gradual replacement of old basement by juvenile crust and associated with subduction zone retreat (rollback), has been documented in some other micro-continents of the CAOB. The preservation of juvenile/mixed crust requires some continental margins that did not collide with any ancient micro-continent or craton (i.e., non-collisional or soft-collisional margins) even until the termination of accretionary orogenesis. The development of a series of oroclines is likely the principal mechanism resulting in survival (preservation) of juvenile/mixed crust within the huge fossil orogen.

1. Introduction

Clarification of the large-scale spatio-temporal distribution of various (juvenile, reworked, ancient) crusts and understanding of geologic processes controlling the crust formation is one of the major subjects of geologic studies and is also extremely important in mineral exploration and prospecting (Hou et al., 2015; Champion and Huston, 2016; Deng et al., 2018). Accretionary (or Pacific-type) orogens, produced by continuing subduction and accretion (Cawood et al., 2009; Condie, 2007), are regarded as Earth's principal sites of continental growth

* Corresponding author.
E-mail addresses: huanghecugb@126.com (H. Huang), taowang@pku.edu.cn (T. Wang).

https://doi.org/10.1016/j.earscirev.2020.103255
Received 18 February 2020; Received in revised form 10 June 2020; Accepted 15 June 2020
Available online 27 June 2020

(Maruyama et al., 1996; Santosh et al., 2010; Safonova, 2017). As exemplified by modern western Pacific and Andes (Cawood et al., 2009; Condie, 2007), there exist two efficient mechanisms resulting in the continental growth in accretionary orogenic systems: 1) the lateral continental growth by accretion of juvenile oceanic arcs, oceanic plateaus, and subduction–accretion complexes, and 2) the vertical growth by magmatic underplating of mantle-derived materials (Jahn et al., 2000a, 2000b; Kemp et al., 2009; Safonova and Santosh, 2014). In long-lived accretionary orogens, the juvenile crust can be then recycled at convergent margins by andesitic to felsic magmatism in continental arcs and by collision-related felsic magmatism (Safonova, 2017). These processes can transport juvenile materials to the relatively shallow crust and might be fundamental to the differentiation, stabilization, and preservation of newly formed continental crust.

As represented by the Andes and western Pacific, respectively (Royden, 1993; Cawood et al., 2009), accretionary orogens can be further subdivided into advancing and retreating types. The former, characterized by advancing of the overriding plate toward the downgoing slab, tends to induce crustal thickening, anatexis, and formation of retro-arc foreland basins (Collins, 2002). In contrast, the latter marked by slab rollback tend to cause crustal thinning, arc splitting, and development of arc-back-arc systems (Cawood et al., 2009). Tectonic switching between these two types of accretionary systems has been frequently documented in the geological history (e.g., Collins, 2002; Jenkins et al., 2002; Lister and Forster, 2009; Cawood et al., 2009; Kemp et al., 2009; Nelson and Cottle, 2017). Recognizing details of such tectonic switching in an ancient accretionary orogen is crucial for unveiling the continental reworking/growth and associated orogenic history.

Zircon Hf isotope of felsic rocks is a powerful tool to trace the nature of sources of felsic magmas. In most natural cases, the isotope results may reflect the mixture of various sources in open systems, e.g., a mix between pre-existing juvenile and older crustal sources or a mix between mantle- and crust-derived magmas. Thus, on a regional scale, felsic igneous rocks can provide information on the distribution of juvenile, ancient and mixed components in deep, unexposed portions of the crust (e.g., Kovalenko et al., 2004; Jung et al., 2009; Wang et al., 2009a; Song et al., 2019). Looking at both secular changes and spatial variations of isotopic signatures, i.e., changes in epsilon values/crustal model ages through time and space, is capable of probing lithospheric architecture and continental growth history (e.g., Hou et al., 2015; Wang et al., 2016; Champion and Huston, 2016; Deng et al., 2018). Moreover, zircon Hf isotope, coupled with whole-rock geochemical data, also has potential for recognizing trench retreat and advance (e.g., Kemp et al., 2009; Nelson and Cottle, 2017) and distinguishing between external and internal orogenic systems (e.g., Collins et al., 2011; Huang et al., 2019b) in ancient accretionary orogens.

The amalgamation history and crustal evolution in the Central Asian Orogenic Belt (CAOB) has been one of the focal themes in the recent years (e.g., Wilhem et al., 2012; Windley et al., 2007; Xiao et al., 2013, 2014, 2020; Zhou and Wilde, 2013; Kröner et al., 2014, 2017; Xiao and Santosh, 2014). The preserved part of the CAOB records long-lived and complex subduction of oceanic lithosphere and amalgamation of various tectonic domains such as accretionary complexes, magmatic arcs, back-arc domains, ophiolitic mélanges, and possibly oceanic plateaus and continental fragments. As the largest Phanerozoic accretionary collages worldwide, the CAOB has been long-term considered to represent an essential site of Phanerozoic continental crustal growth (Chen and Arakawa, 2005; Han et al., 1997; Jahn et al., 2000a, 2000b, Jahn, 2004). However, some groups of geologists proposed that 1) the involvement of ancient continental crust during the evolution of the CAOB has been underestimated, and 2) much of the vertical juvenile growth in Central Asia occurred after the completion of the accretionary orogenesis (e.g., Kröner et al., 2014, 2017). Therefore, whether extensive juvenile additions associated with accretionary orogenesis occurred and, if any, are still preserved in the CAOB is a pending issue.

Micro-continents with Precambrian crystalline basements constitute a large proportion of the CAOB crust, and controlled the overall geometry of the intervening sutures and acted as nuclei for accretionary crustal growth (Zhou et al., 2018). They were extensively overprinted by Phanerozoic tectonism, magmatism, and metamorphism. To clarify the distribution of the juvenile, ancient, and mixed crustal components within these micro-continents is critical for the overall evaluation of the Phanerozoic continental crustal growth in the CAOB. The Yili Block is one of the continental fragments with a Precambrian basement in the SW CAOB (Wang et al., 2014a, 2014b), and its southern and northern margins acted as ancient convergent plate margins beneath which Paleo-Asian oceanic lithosphere was subducted (Long et al., 2011; Han and Zhao, 2018). A remarkable feature of the Yili Block and its adjacent regions is the development of the widespread Paleozoic granitoid intrusions and their volcanic counterparts. Previous studies have reported a large number of geochronologic, geochemical, and isotopic data. Therefore, the Yili Block is an ideal natural laboratory to study the formation and distribution of various types of crust in the micro-continents of the CAOB and other scientific issues. In this contribution, we present a comprehensive synthesis of information from the Paleozoic felsic rocks in the Yili Block and adjacent regions, including their spatial and temporal distribution, whole-rock major and trace elemental and Nd-isotopic characteristics, and zircon Hf isotopic compositions. The results enable us to offer perspectives on the lithospheric architecture of the Yili Block and adjacent regions and thus monitor crustal evolution to micro-continents in the context of CAOB evolution. This compilation may provide us with a better understanding of the geodynamic control on growth and reworking of the crust as well as the preservation of juvenile components in micro-continents during accretionary orogenesis.

2. Geological framework

The Tianshan (or Tien Shan, Tienshan), located in the SW CAOB and extending for more than 2500 km from Uzbekistan to SW Mongolia (Fig. 1b), is a composite collage geologically comprising a series of micro-continents and intervening accretionary complexes. The Chinese Tianshan is subdivided into Eastern Tianshan and Western Tianshan roughly separated by longitude ~88°E or by Tuokexun–Kumishi High Road (Fig. 1b; Gao et al., 2009; Li et al., 2006), which distinctly differ in topography and Paleozoic tectonic evolution (e.g., Chen et al., 1999a; Xiao et al., 2013; Zhang et al., 2016a). The present study focuses on the Yili Block and adjacent regions located in the Chinese Western Tianshan. Major faults, ophiolite belts, and (U)HP metamorphic rocks separate the Chinese Western Tianshan and adjacent regions into several tectonic domains, i.e., the northern margin of Tarim Craton, South Tianshan Belt, Chinese Central Tianshan Block, Yili Block and Chinese North Tianshan Belt (Fig. 1c).

The northern margin of Tarim Craton (NTC) refers to the exposures between the North Tarim Fault to the north and Takelamagan desert to the south. The Precambrian basement rocks, represented by Neoarchaean TTGs (tonalite-trondhjemite-granodiorite) and granitic gneisses, early Palaeoproterozoic orthogneiss, late Palaeoproterozoic granitoids, and supracrustal rocks, and diverse Neoproterozoic magmatic rocks (Lu et al., 2008; Long et al., 2010, 2012; Shu et al., 2011; Zhang et al., 2013a), are well preserved in the Kuruktag (also spelled Quruqtagh or Kuluketage) area in the northeastern margin of the craton. In the northwestern Tarim Craton, Late Precambrian to Devonian sequences are characterized by shallow marine to nonmarine limestone and sandstone (Carroll et al., 1995; Han et al., 2011), with a widespread unconformity at the Ordovician–Silurian boundary (e.g., Carroll et al., 2001; Ge et al., 2012a; Shi et al., 2007), and are unconformably overlain by the Carboniferous and Permian deposits (Carroll et al., 1995). Small felsic intrusions with emplacement ages from 460 to 400 Ma (peak at ~420 Ma) are well documented in the Kuruktag and nearby regions. Some Early Permian kimberlitic

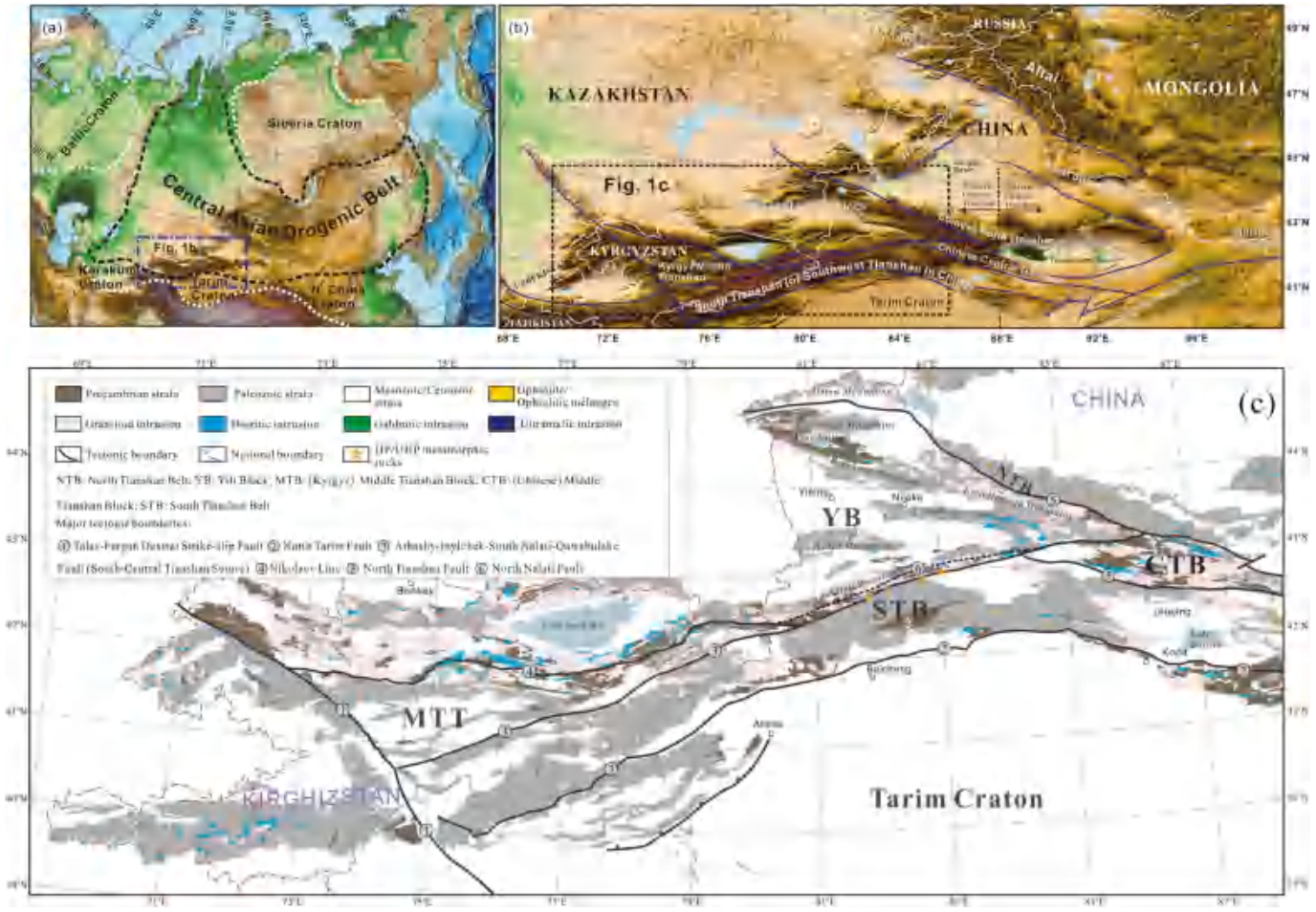

Fig. 1. (a) Topographic features and tectonic overview map of Central Asian Orogenic Belt and adjacent cratons (modified from Sengör et al., 1993; Windley et al., 2007; Xiao et al., 2015; Han and Zhao, 2018; basemap from website http://www.ngdc.noaa.gov/mgg/global). (b) Topographic map and terminology of the of North Xinjiang and adjacent area of the SW Central Asian Orogenic Belt (basemap from website http://www.ngdc.noaa.gov/mgg/global) showing the Altai, Junggar, Tianshan and Northern Tarim segments from north to south. (c) Geological map of the Chinese Western Tianshan (modified after unpublished 1:1,000,000 geological map of Chinese and Kyrgyz Tianshan by Xi'an Center of Geological Survey, China Geological Survey).

intrusions, OIB-like mafic intrusions/basalts, bimodal dykes and syenites/granites occur in the western and central parts of the NTC (Zhang and Zou, 2013a, 2013b; Cheng et al., 2018, and references therein).

Geologically, the Chinese South Tianshan (or Chinese Southwest Tianshan) and Kyrgyz South Tien Shan are parts of one single tectonic belt that is termed South Tianshan Belt (STB) herein. The belt mainly comprises Precambrian basement rocks representing fragments of the NTC, Early Paleozoic arc sequences, and Late Paleozoic volcano-sedimentary sequences. The Precambrian basement rocks of the STB are represented by Palaeoproterozoic Xingditagh and Muzha'erte formations and Mesoproterozoic Akesu Formation, all exposed in the central part of this belt (Xu et al., 2013a; Yang and Zhou, 2009). Ediacaran to Lower Cambrian sedimentary rocks and Middle Ordovician to Early Devonian (~460 to ~410 Ma) continental-arc-type volcanic rocks have a wide occurrence (Han et al., 2011; Xiao et al., 2013, and references therein; Wang et al., 2018d; Zhong et al., 2019). Theses Early Paleozoic strata generally display a low- to medium-grade metamorphic overprint (Wang et al., 2018d). In the northern part of the STB, unmetamorphosed Carboniferous volcano-clastic rocks and limestones unconformably overlie the intensely deformed and weakly metamorphosed Devonian clastic rocks and Silurian schists (Xu et al., 2013a). In the southern part of the STB, the early strata are locally unconformably overlain by early Permian terrestrial volcano-clastic successions (Huang et al., 2015a; Wang et al., 2018d). Two episodes of plutonism have been identified in the STB. Intrusive rocks with Early Palaeozoic ages mainly occur in the eastern segment, and those with Late Carboniferous to Early Permian ages are discontinuously distributed in the entire belt. No post-Permian U–Pb age has been reported from the STB igneous so far (Han et al., 2011). Ophiolitic mélanges formed following the closure of the Paleozoic South Tianshan Ocean occur discontinuously in the STB. The majority of the rocks display Late Ordovician to Middle Devonian ages (Jiang et al., 2014; Wang et al., 2011; Wang et al., 2018d, and references therein).

Separating the ribbon-shaped STB from its northern neighbors (see below), the South Tianshan Suture (Fig. 1c) is marked by W-E trending Atbashy-Inylchek-South Nalati-Qawabulake (AISNQ) fault, a high-pressure and ultrahigh-pressure (HP-UHP) metamorphic complex and associated ophiolitic mélanges. The AISNQ fault is a large-scale Permian strike-slip fault that reworked the earlier suture zone (Charvet et al., 2011; Laurent-Charvet et al., 2002, 2003; Wang et al., 2008, 2009b; Zhu et al., 2018a; Tan et al., 2019). The HP-UHP metamorphic complex consists mainly of blueschist-, eclogite-, and greenschist-facies meta-sedimentary rocks, and some mafic metavolcanic rocks with N-MORB, E-MORB, OIB and arc basalt affinities (Gao and Klemd, 2003; Gao et al., 2011; Gao et al., 1998; Zhang et al., 2013b).

North of the South Tianshan Suture are juxtaposed micro-continental blocks, including the Kyrgyz Middle Tianshan, Yili, and Chinese Central Tianshan blocks (abbreviated as KMTB, YB, and CCTB, respectively). The tectonic division scheme applied in the present work is shown in Fig. 1c. We do not follow the scheme that the Nikolaev Line

in Kyrgyzstan (the major fault with no. 4 in Fig. 1c), the northern border of the KMTB, continues eastward into China and join the North Nalati Fault (the major fault with no. 6 in Fig. 1c). According to such a scheme, the KMTB could thereby be connected to the CCTB through the southernmost margin of the "Yili Block" referred to in this study (e.g., Long et al., 2011; Han and Zhao, 2018; Gao et al., 2009; Qian et al., 2007). Alternatively, we consider that the Nikolaev line terminate close to the China-Kyrgyzstan border (see details in Section 7.1).

The Yili Block, a triangle-shaped area that wedges out eastwards, belongs to the gigantic Kazakhstan-Yili Continent and constitutes the southern limb of the Kazakhstan Orocline. The central part of the Yili block is covered by thick Mesozoic to Cenozoic sedimentary sequences (Fig. 1b and c) and is therefore termed as "Yili Basin". The pre-Mesozoic rocks are preserved in some topographic highlands, i.e., from north to south, Biezhentao, Borohoro-Eren Habirga, Awulale, Wusun, and Nalati mountains (Fig. 1c). In the northwestern YB, the Precambrian basement rocks occur mainly around the Lake Sailimu (Hu et al., 2010; Wang et al., 2014a, 2014b), and consist mainly of gneissic granites, migmatites, high grade meta-sedimentary, and meta-volcanic rocks (Hu et al., 2000, 2010; Wang et al., 2014a, 2014b; Zhu et al., 2019). Formation ages of ~926 to ~845 Ma were reported for migmatites and gneissic S-type granites (Wang et al., 2014b). The basement rocks of the southern Yili Block mainly occur along the northern slope of the Nalati mountains. They are composed mainly of amphibolite facies metamorphic rocks, a low-grade series of quartz schist and sericite-chlorite-phyllite interlayered with quartzite and crystalline carbonate, and low-grade metasedimentary rocks (XBGMR, 1993; Zhu et al., 2019, and references therein). Precise ages for these rocks are scarce, and only few gneissic granites were dated at early Neoproterozoic (e.g., Chen et al., 1999b; Hu et al., 2000; Zhu et al., 2019). The Precambrian affinity is still a topic of debate. The proposed potential orgin of the YB include the Tarim (e.g., Rojas-Agramonte et al., 2011; Shu et al., 2011; Ma et al., 2012; Wang et al., 2014a), Baltica (East Gondwana) (e.g., He et al., 2018; Huang et al., 2019b), Siberia, and North China cratons (see Zhu et al., 2019, and references therein). Unconformably overlying these basement rocks are thick Paleozoic volcanic and sedimentary sequences (XBGMR, 1993; Bao et al., 2018). Early Paleozoic strata consist of Cambrian to Ordovician carbonates and clastic rocks and Silurian flysch in the north of the Yining area (XBGMR, 1993; Wang et al., 2014a, 2014b). Late Paleozoic sequences consist mainly of Devonian terrigenous rocks, and Carboniferous sandstones, limestones intercalated with pyroclastic and volcanic rocks. Permian formations consist of conglomerates and terrestrial sandstones, unconformably overlying the older rocks (Wang et al., 2009b; XBGMR, 1993). Igneous rocks have a widespread occurrence in the YB and constitute two igneous belts respectively roughly parallel to inferred northern and southern suture zones (Fig. 1c).

The Chinese Central Tianshan Block is a strip-like continental block that extends from the Baluntai area in the Western Tianshan to the Xingxingxia area in the Eastern Tianshan. The CCTB consists of several distinguishable petrotectonic assemblages including, from oldest to youngest, (a) Proterozoic basement composed of Meso- to Neo-proterozoic schists, paragneiss and granitic gneisses (Yang et al., 2006; Chen et al., 2009; Hu et al., 2010; Lei et al., 2011; He et al., 2014; Wang et al., 2014a, 2014b; Wang et al., 2017; Huang et al., 2017a; He et al., 2018), (b) Ordovician–Early Devonian arc-related volcanic rocks and intrusions and (c) unconformably-overlying Carboniferous and post-Carboniferous sedimentary cover (Shu et al., 2002; Wang et al., 2011; Ma et al., 2015). Late Carboniferous to Permian non-deformed intrusive rocks crosscut the pre-Carboniferous rocks (Ma et al., 2014; Zhong et al., 2015; Huang et al., 2015b; Yin et al., 2017).

The North Tianshan Belt is separated from Yili and Central Tianshan blocks by the North Tianshan Suture (Fig. 1b and c). The suture zone contains the North Tianshan Fault along which high-pressure glaucophane-phengite schists and ophiolitic fragments occur (Wang et al., 2006; Xiao et al., 2013, and references therein). The ophiolitic fragments crop out discontinuously for about 200 km (Fig. 1c). Zircon U-Pb ages of 324.8 ± 7.1 Ma and 344.0 ± 3.4 Ma were reported for plagiogranite and gabbro, respectively, from the Bayingou region (Xu et al., 2006), and ages of 343.1 ± 2.7Ma for plagiogranite from the Luweigou region (Li et al., 2015a). Along with the suture zone, exposed rocks are composed mainly of Devonian tuffaceous sandstone, tuff, slate, phyllite, limestone and intermediate-mafic volcanic rocks, Lower Carboniferous rhythmic tuffaceous siltstones and Upper Carboniferous clastic and pyroclastic rocks, and are widely viewed as components of an accretionary complex (Xiao et al., 2013; Han et al., 2010; Feng and Zhu, 2018).

3. Paleozoic felsic magmatism in the Chinese Western Tianshan

Field work was conducted in the Yili Block, and some samples were collected from Paleozoic granitoid plutons in both northern and southern magmatic belts. In addition, we compile up-to-date U-Pb age, zircon Hf isotopic, and whole-rock major and trace elemental and Nd isotopic data of felsic rocks in the Western Tianshan from the literature. Intrusions and volcanic suites dominated by rocks with $SiO_2 < 60$ wt.% are mostly filtrated; however, some rocks with 57–60 wt.% SiO_2 are retained because they are exposed in areas where few coeval felsic rocks are preserved. The analytical methods for whole-rock major and trace elemental as well as zircon U-Pb and Hf isotopic analysis, cathodoluminescence (CL) images for zircon grains presently analyzed, and newly acquired U-Pb isotopic results are together included in Supplementary Material 1. Location, general petrographic, geochronological, zircon Hf isotopic, and whole-rock geochemical features of individual granitoid plutons/felsic volcanic suites are summarized in Table S2.1 in Supplementary Material 2. New and compiled zircon Hf isotopic data, and whole-rock element [major and trace (including rare earth) elements] and Nd isotopic concentrations for felsic rocks are presented in tables S2.2 and S2.3 in Supplementary Material 2, respectively. These rocks are mostly granitoids with a few rhyolites and dacites. Based on their geochemical signatures, felsic rocks are broadly subdivided into the following five types: I-type, adakite-like, S-type, A-type, and highly fractionated. We caution that the notation is used below in a non-genetic sense to convey the general characters of individual granitoid intrusions and felsic volcanic units. The general characteristics in major and trace elements for these rocks are illustrated in figures in Supplementary Material 3.

The Paleozoic magmatic rocks form several magmatic belts generally extend parallel to inferred major sutures, implying that the formation of the Paleozoic igneous rocks was mostly associated with the consumption of branches of the Paleo-Asian Ocean. A ~497 Ma biotite monzonitic granite intrusion was reported from the southern margin of the YB (SY-11 in Fig. 2a; Xu et al., 2013b). In addition to this, Ordovician granitoid intrusions sporadically occur along major sutures (Fig. 2a). These rocks are dominated by calcic-alkalic to alkalic-calcic I-type granitoids with minor S-type granitoids (e.g., NY02 in Fig. 2a).

Few Silurian and Early Devonian rocks have been recognized on the northern margin of the YB so far (e.g., NY03 in Fig. 2a). On the southern margin of the YB, the Silurian and Early Devonian magmatism was likely the continuation of Ordovician magmatism, and is represented by discontinuously exposed normal I-type (e.g., SY02, 05, 06, 09, 12, 49 in Fig. 2a), adakite-like (e.g., SY03 and 07 in Fig. 2a) and A-type (e.g., SY13 in Fig. 2a) granitoids. In the western section of the CCTB, the preserved Silurian to Early Devonian felsic plutonic rocks mostly exhibit the petrological and geochemical features of I-type granitoids (Ma et al., 2014). The Silurian and Early Devonian I-type granitoids and dacites, with few highly fractionated rocks (e.g., ST09 in Fig. 2a), also occur in the eastern segment of the STB, and the plutonic rocks mostly intruded the basement rocks that are likely parts of the Tarim basement in the southern part of the STB. The above facts suggest that these Early Palaeozoic igneous rocks exposed in the present STB were initially emplaced in the northern margin of Palaeozoic Tarim (Ge et al., 2014,

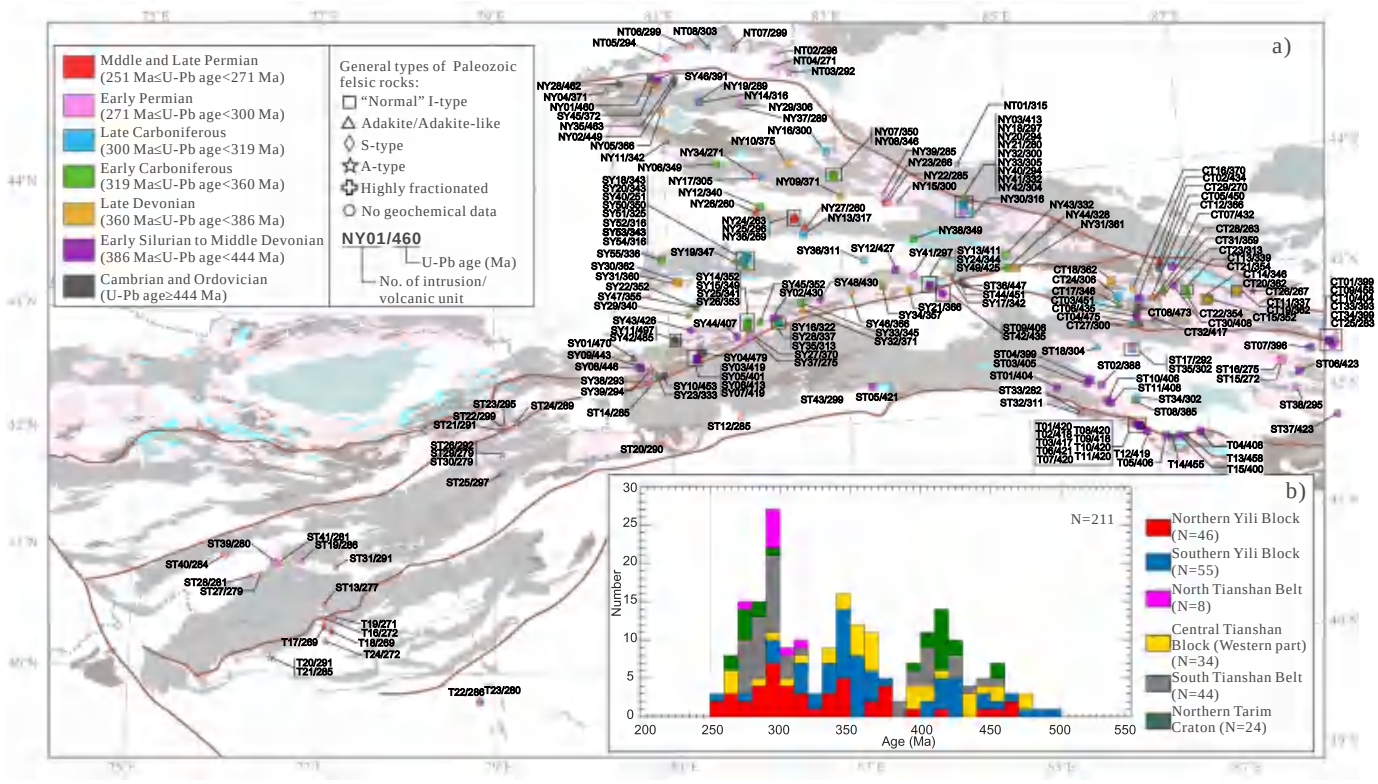

Fig. 2. (a) Geological map of the Chinese Western Tianshan showing ages and types of most Paleozoic granitoid intrusions and felsic volcanic suites. See Table S2.1 in Supplementary Material 2 for data sources and other details. (b) Histogram of zircon U-Pb ages for Paleozoic from major tectonomagmatic belts of the Chinese West Tianshan. See Table S 2.1 in Supplementary Material 2 for data sources and details

2012b; Huang et al., 2013, 2019a). In the NTC, Silurian felsic intrusions temporally peaked at ~420 Ma (Fig. 2b) are predominately preserved in the Kuruktag and nearby regions. They are dominated by normal calc-alkaline, I-type granitoids with sporadic adakite-like rocks (e.g., T02 in Fig. 2a).

There seems to be a ~20 My (~395 Ma to ~375 Ma) period of magmatic quiescence in the Chinese Western Tianshan (Huang et al., 2019a), given the rare magmatic record during this period except for some I-type rocks in the STB (e.g., ST02, 08 in Fig. 2a) and northern YB (NY46 in Fig. 2a). Subsequently, the magmatism recommenced in the Late Devonian, as recorded by voluminous Late Devonian to Early Carboniferous magmatic rocks in the YB and CCTB. In the northern part of the YB, ~375 to ~340 Ma granitoids are mainly show features of calc-alkaline, I-type granitoids, and a few Early Carboniferous adakites or adakite-like rocks (e.g., NY05 in Fig. 2a) (always spatially and temporally associated with high Mg andesites) and A-type granites (e.g., NY04 and NY11 in Fig. 2a) are locally exposed. The period between Late Carboniferous and Early Carboniferous (~340 to ~320 Ma) was previously thought as a magmatic quiescent period. However, recent recognition of some granitoids formed during this period (e.g., NY41, 43, 44 in Fig. 2a) (Wang et al., 2018a), coupled with the abundance of 320–340 Ma igneous ages for detrital zircons from forearc turbidites from the accretionary complex of the North Tianshan Belt (Wang et al., 2018b, Fig. 7b), argues against a magmatic hiatus in the northern YB during the late Early Carboniferous.

In the southern part of the YB, this episode of magmatism, lasting until the latest Early Carboniferous (~320 Ma), is characterized by widespread emplacement of calc-alkaline, I-type granite, with subordinate A-type and adakite-like rocks. Besides, an Early Carboniferous (ST23 in Fig. 2a) S-type granite intrusion is exposed close to the China-Kazakh border. In the western part of the CCTB, the exposed ~370 to ~337 Ma granitoids predominately show a calc-alkaline, I-type affinity, with a few intrusions being of adakite-like (CT15, 17, 21 and 22 in Fig. 2a) and A-type (CT12 in Fig. 2a) granite.

Late Carboniferous felsic rocks are sporadic in the Western Tianshan. In the YB and CCTB, they are composed of I-type, adakite-like, A-type, and highly fractionated felsic rocks. An ~315 Ma and two 300 Ma (NT01, 07, and 08 in Fig. 2a) A-type granitic intrusion was reported from the North Tianshan Belt (NTB) (Wang et al., 2018e). After ~60 My magmatic quiescence, the magmatism re-occurred in the South Tianshan Belt (STB), as recorded by emplacement of I- (ST34 in Fig. 2a), adakite-like (ST18 and 35 in Fig. 2a) and A-type (ST32 in Fig. 2a) granitoids in the eastern part of the belt.

Permian felsic rocks occur throughout the whole Chinese Western Tianshan and are variable in type. Compared with earlier magmatism, the typical characteristic of the Permian felsic magmatism is the large area proportion of A-type granites in all exposed Permian felsic rocks (Figs. 2a and 3, and Supplementary Material 2) (Long et al., 2011; Tang et al., 2017a). The A-type granites, with ages ranging from ~300 to ~269 Ma, were mainly emplaced in the northern Tarim Craton (NTC), western STB and NTB, and are sporadically exposed in other areas. Permian I-type granitoids have a widespread occurrence in the YB, CCTB and STB. Adakite-like granitoids are distributed in the Awulale mountains (~296 Ma, NY25, 26, 27 in Fig. 2a) of the northern YB, and in the Chuanwulu area of the western STB (~286 Ma, ST19 in Fig. 2a). Besides, a few S-type granitoids and rhyolites were reported from the STB (e.g., ST14, 20, 33, 43 in Fig. 2a).

4. Secular whole-rock elemental variations in the Yili Block and adjacent regions

Several geochemical indices of crust-derived felsic rocks, such as Sr/Y and Sr/Yb are sensitive to high-pressure minerals (i.e., amphibole and garnet) and, despite some exceptions, statistically increase with increasing pressures (crustal depths) under which melt generation took place (Chapman et al., 2015; Ge et al., 2014; Mamani et al., 2010;

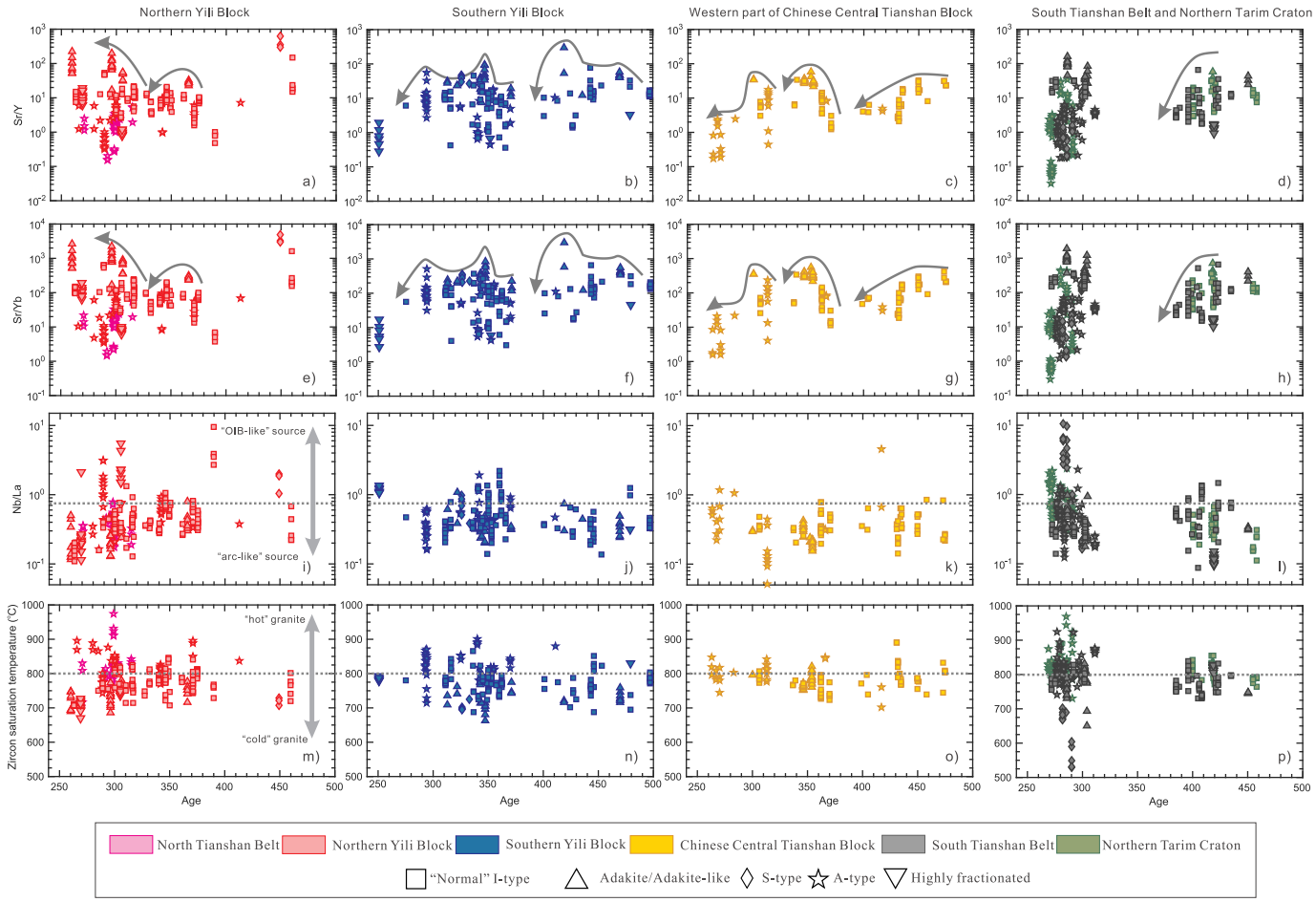

Fig. 3. Trace elements ratio and zircon saturation temperature (Watson and Harrison, 1983) versus crystallization age of Paleozoic felsic rocks of the West Tianshan. Data used for plot are listed in Table S2.3 in Supplementary Material 2.

Profeta et al., 2015; Zhang et al., 2018). The maximum high-pressure mineral abundance in the residue roughly provides a minimum constraint on melting depth and, on a regional-scale, crustal thickness. The Nb/La ratio is another important index for genesis and tectonic settings of felsic rocks, since high ratios (e.g., > 0.71) are likely indictive of high-degree involvement of ocean island basalts (OIB)-like sources generally associated with lithospheric extensional settings (Sun and McDonough, 1989; Rudnick, 1995), whereas low (e.g., < 0.71) probably reflect "arc-like" or "crust-like" sources (Pearce and Peate, 1995; Condie, 1999; Tang et al., 2017a). We emphasize that the above assumptions are a simplification and only statistically valid, and generally work for studies on a large scale. In addition, although shown on the plots, the aforementioned ratios of S-type and highly fractionated granites are excluded when summarizing the long-term elemental variations, given the complexity of their sources.

Late Silurian to Early Devonian (~420 to ~400 Ma) felsic magmatism the southern YB, CCTB, and STB-Northern Tarim exists general decreasing trends in Sr/Y and Sr/Yb (Fig. 3b–d and f–h). After a ~20 My (~395 Ma to ~375 Ma) period of magmatic quiescence, the recommencement of felsic magmatism in the YB and CCTB is characterized by an episode (~375 to ~350 Ma) of increasing trends in Sr/Y and Sr/Yb ratios, and a following interval (~350 to ~330 Ma) of decreasing trends (Fig. 3a–c and e–g). Between ~320 to ~300 Ma, Sr/Yb and Sr/Y ratios of felsic rocks from the northern YB increase with decreasing age (Fig. 3a and e). The occurrence of high Sr/Y and Sr/Yb felsic rocks during ~300 to ~295 Ma is a common feature for all magmatic belts (Fig. 3a–h). Then, with few exceptions (e.g., NY26 in Fig. 2a) in the Awulale Mountains of the northern YB, the low Sr/Y and Sr/Yb felsic magmatism gradually took advantage in the entire Chinese Western Tianshan, until the end of the Paleozoic magmatism at ~250 Ma (Fig. 3a–h). Besides, the up-to-date dataset reveal some pulses of emplacement/eruption of high Nb/La felsic rocks for Chinese Western Tianshan, i.e., ~410 to ~400 Ma in the STB, ~370 to ~340 Ma in the northern and southern parts of the YB, ~310 to ~290 Ma in the northern YB and ~290 to ~270 Ma in the northern Tarim Craton (Fig. 3i–l).

5. Spatial and temporal Hf-isotope variations in the Yili Block and adjacent regions

A total of 2250 zircon grains from 113 granitoid plutons/felsic volcanic suites in the West Tianshan are compiled to infer their evolution through time and the spatial extent of "crustal blocks" of specific Hf isotope character. Relative abundances of crustal Hf model ages (T_{DM}^{C}) for autocrystic zircon grains (xenocrystic zircons, outliers in autocrystic zircons and zircons with U-Pb ages being reset in each sample are not included, similarly hereinafter) in each sample are illustrated as pie charts in Fig. 4a, and different colors of frames of these pie charts are used to distinguish their crystallization ages. A comparison between median T_{DM}^{C} values and regional magnetic anomalies is illustrated in Fig. 4b.

For some areas where Hf isotopic data density is high, the crustal Hf model age contour map (Fig. 5a) was produced in ArcGIS using the inverse distance weighted interpolation method as described by Mole et al. (2014). This method used 12 nearest neighbors at a "power" of 2 in the Geostatistical Analyst modeling feature of ArcGIS, which

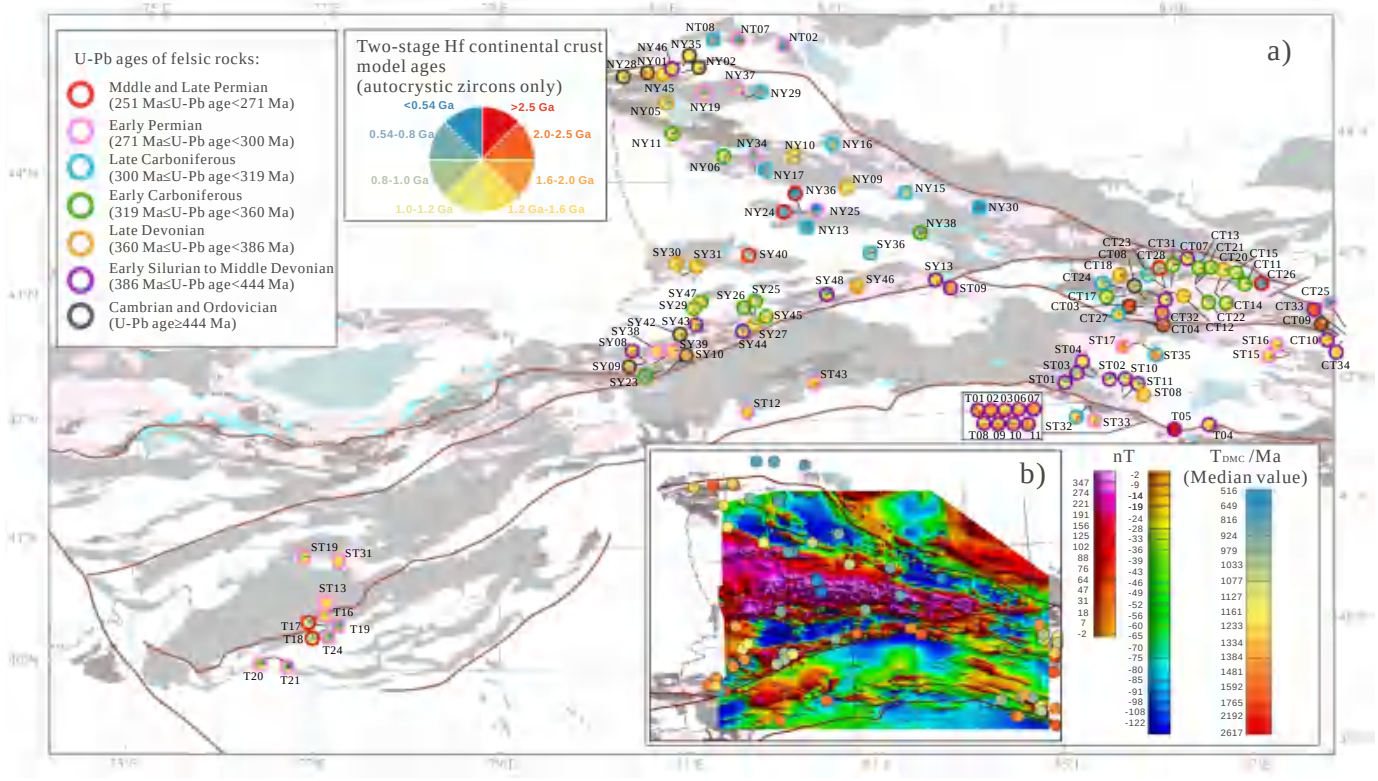

Fig. 4. (a) Map of Hf model ages for felsic rocks of the West Tianshan, showing relative abundances of crustal Hf model ages (T_{DM}^{C}) for autocrystic zircon grains in each pluton/volcanic suite (illustrated as pie charts). (b) The magnetic anomaly map of the Yili Blcok and adjacent regions, showing median T_{DM}^{C} value. The magnetic anomaly map is from Yu (2016) and high-resolution image files are provided by the author personally. Data are from this study and literature. See Table S2.1 in Supplementary Material 2 for data sources and details and Table S2.2 in Supplementary Material 2 for original zircon Hf isotopic data.

accounts for the distance between sample points in the most representative manner (Mole et al., 2014). All Hf isotope data were grouped by the geometric interval method designated for class breaks in ArcMap, which ensures that each class range has approximately the same number of values and that the change between intervals is relatively consistent. All point data shown in the contour maps represent the median value of T_{DM}^{C} of autocrystic zircons from individual rock samples (outliers were removed). One orogen-transverse profile of zircon crustal Hf model ages, across the North Tianshan Belt and the Yili Block, is presented in Fig. 5b. For Paleozoic felsic rocks in the Yili Block, relative abundances of T_{DM}^{C} for autocrystic zircon grains, together with general rock types, of each intrusion/volcanic suite are also displayed on the plot of U-Pb rock age versus distance to the suture (Fig. 6). The variations in zircon Hf isotope with crystallization ages are illustrated in Figs. 7 and 8, and histograms of crustal Hf model ages (T_{DM}^{C}) of autocrystic and xenocrystic zircons are illustrated in Supplementary Material 4)

5.1. Late Cambrian to Middle Devonian magmatism

A few Late Cambrian to Early Silurian (~493 to ~441 Ma) autocrystic zircon grains were reported for the northern Yili Block. The εHf(t) ranges from −3.88 to +4.53 and the crustal Hf model ages (T_{DM}^{C}) from 1.16 to 1.69 Ga (Fig. 7b). One Middle Devonian intrusion (NY 46 in Fig. 2a) exposed in the northern YB show εHf(t) varying from −0.59 to +5.33 and T_{DM}^{C} from 1.05 to 1.43 Ga. In the southern YB, the Middle Cambrian to Late Ordovician (~502 to ~444 Ma) autocrystic zircons show similar zircon Hf isotopic characteristics, with εHf(t) varying from −5.16 to +9.48 and T_{DM}^{C} from 0.82 to 1.77 Ga (Fig. 7c). Subsequently, ~443 to ~389 Ma felsic magmatism in the southern YB shows the Hf isotopic pull-up, as exhibited by overall higher and more variable εHf(t) values of −7.44 to +15.19 and corresponding relatively younger T_{DM}^{C} of 0.45 to 1.90 Ga (Fig. 7c). Spatially, the rocks mentioned above generally define some small-scale low εHf(t)/old T_{DM}^{C} domains immediately adjacent to the northern and southern sutures of the Yili Block (Fig. 4a).

During the Early Paleozoic (~477 to ~393 Ma), the granitoid magmatism occurring in the western part of the Chinese Central Tianshan Block is characterized by a remarkable heterogeneity in zircon Hf isotope, with two groups of εHf(t) values ranging from −17.09 to −3.73 (T_{DM}^{C} = 1.64–2.51 Ga) and from −1.54 to 9.52 (T_{DM}^{C} = 0.85–1.49 Ga), respectively (Fig. 7d). Rocks of the former group are exposed in narrow areas of the southern margin of the CCTB, whereas ones of the latter group are found in central and northern parts (Fig. 4a).

The up-to-date zircon Hf isotopic results for Early Paleozoic felsic magmatism in the South Tianshan Belt indicate the involvement of both juvenile and ancient components. The εHf(t) values for 432 to 375 autocrystic zircons, predominately contained by felsic rocks preserved in the eastern section of the belt, range from −8.37 to +13.18 and T_{DM}^{C} from 0.54 to 1.93 Ga (Fig. 7e). In contrast, Early Paleozoic (434–406 Ma) granitoids from the Kuruktag and nearby areas of the northern Tarim Craton are featured with ancient zircon Hf isotopic compositions (Fig. 7e). One Late Silurian monzogranite intrusion (T05) yields εHf(t) ranging from −23.12 to −16.25 and T_{DM}^{C} from 2.42 to 2.85 Ga, which defines the most ancient source of the Paleozoic felsic rocks of the West Tianshan (Fig. 4a). Other felsic rocks show εHf(t) varying from −13.85 to +1.71 and T_{DM}^{C} from 1.29 to 2.28 Ga (Figs. 4a and 7e).

5.2. Late Devonian to Late Permian magmatism

Late Devonian to early Early Carboniferous (~384 to ~335 Ma) granitoids in the northern YB display εHf(t) values ranging from −1.69

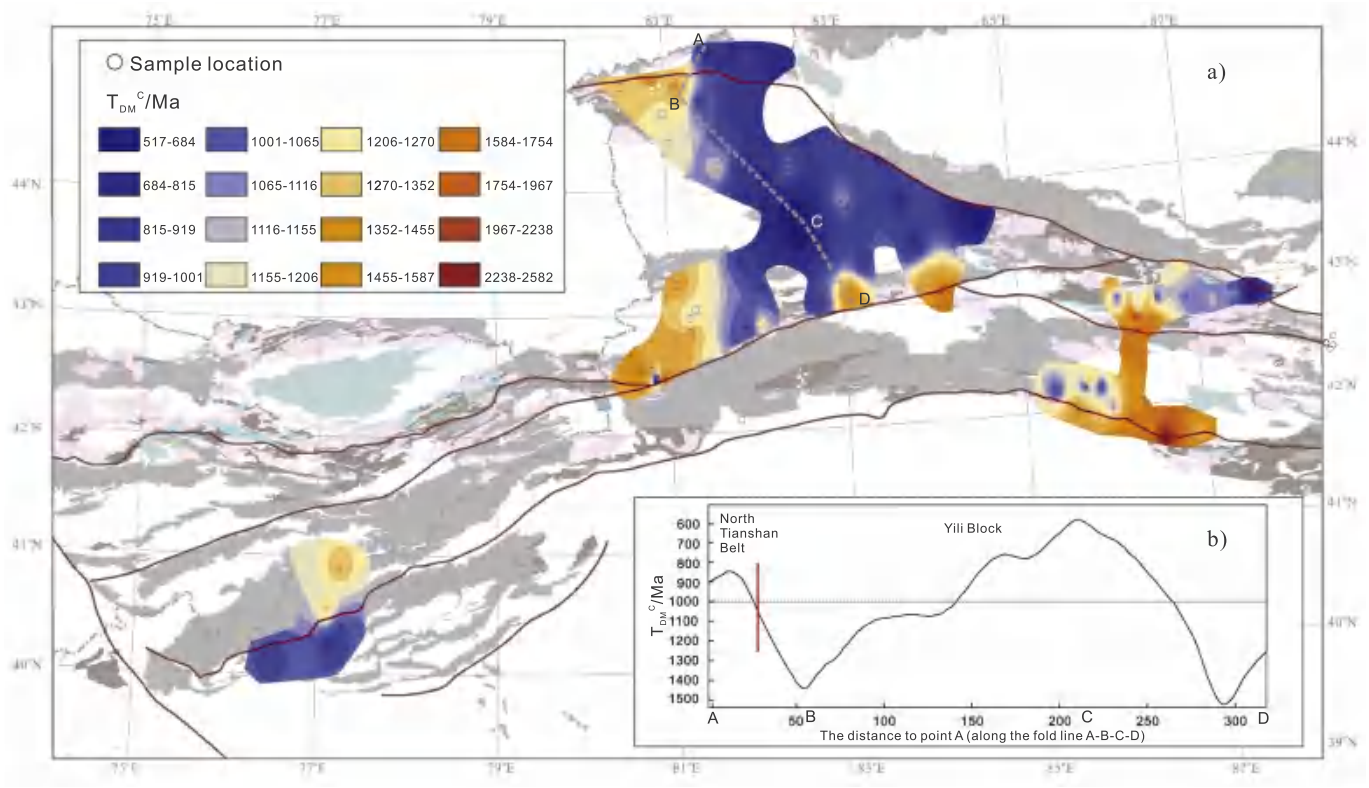

Fig. 5. (a) Hf isotope contour map showing the spatial variation of crustal Hf model ages for the Paleozoic granitoid rocks and felsic volcanic rocks in some areas of the West Tianshan. ABCD marks a transect onto which zircon Hf model age variations were projected in Fig. 7b. (b) Cross section of Hf isotopic data (T_{DM}^{C}) across the North Tianshan Belt and the Yili Block. See Table S2.1 in Supplementary Material 2 for data sources and details and Table S2.2 in Supplementary Material 2 for original zircon Hf isotopic data.

to +14.17 and T_{DM}^{C} from 0.44 to 1.46 Ga, and a downward to upward transition can be observed around 350 Ma (Fig. 7b). According to their median T_{DM}^{C} values (1.20–0.88 Ga), these granitoid intrusions mostly constitute domains of "mixed" to "slightly juvenile" Hf isotope in Borohoro-Eren Habirga mountains (Fig. 4a). Subsequently, felsic rocks in the northern YB show a shift of εHf to more isotopically depleted values at ca. 335 Ma, as suggested by positive εHf(t) (*t* ranges from ~335 to ~300 Ma) values of +3.42 to +15.29 and juvenile T_{DM}^{C} of 0.35–1.11 Ga (Fig. 7b). Permian autocrystic zircons consistently exhibit positive εHf(t) values (+3.46 to +13.62) and relatively juvenile T_{DM}^{C} (0.42–1.08 Ga) (Fig. 7b). Together, several domains with very "juvenile" Hf isotopic compositions in the northern YB are outlined by these Late Carboniferous and Permian felsic rocks (Fig. 4a).

In the southern YB, Hf isotopic pattern of 380–335 Ma autocrystic zircons is characterized by the large variation in εHf(t) (−8.19 to +8.06) and T_{DM}^{C} (0.84–1.81 Ga) (Fig. 7c), and the shift in the evolutionary trend from upward to downward occurred at ~350 Ma (Fig. 7c). Spatially, felsic rocks emplaced during this period constitute two old T_{DM}^{C} domains (~1.4 to ~1.6 Ga) in the Wusun Mountain and the middle Nalati Mountains, respectively, and a "mixed" to "slightly juvenile" T_{DM}^{C} (~1.0 to ~1.2 Ga) domain south of the Nileke County (Figs. 4a and 5a). One granitoid intrusion (SY36) exposed south of Xinyuan County display εHf(t) (*t* ranges from 301 to 318 Ma) and T_{DM}^{C} varying from +3.95 to +9.86 and from 0.70 to 1.07 Ga, respectively (Fig. 4a). Up-to-date reported Early Permian autocrystic zircons are contained by granitoids cropping out close to the China-Kyrgyzstan border and are characterized by moderately ancient Hf isotope [εHf(t) = −4.53 to +2.78 and T_{DM}^{C} = 1.14–1.60 Ga] (Figs. 4a and 7c). Late Permian autocrystic zircons are reported from a highly fractionated granite intrusion in the eastern Wusun Mountains, north of Nileke County (Fig. 4a). They display εHf(t) (*t* ranges from 250 to 262 Ma) of +2.88 to +6.60 and T_{DM}^{C} of 0.87 to 1.10 Ga (Fig. 7c).

In the western CCTB, the overall Hf isotopic pull-up is exhibited by Late Devonian to Early Carboniferous granitoids, as εHf(t) increases from −7.88 to +10.15 for ~370 to ~350 Ma autocrystic zircons (corresponding T_{DM}^{C} = 0.72–1.87 Ga) to +0.11 to +7.93 (corresponding T_{DM}^{C} = 0.84–1.34 Ga) for ~349 to ~323 Ma ones (Fig. 7d). The Late Carboniferous (~319 to ~300 Ma) granitoids reported from the western CCTB show Hf isotopic features comparable to that of Early Carboniferous ones [εHf(t) = −1.06 to +7.36 and T_{DM}^{C} = 0.86–1.39 Ga], and Permian autocrystic zircons show more juvenile Hf isotopic features, with εHf(t) of +4.31 to +12.86 and T_{DM}^{C} of 0.47–1.02 Ga. Spatially, a general northeastward younging trend in Hf isotope is recorded by these Late Paleozoic granitoids in the western CCTB (Fig. 7d).

As mentioned, in addition to those occurring in micro-continents of YB and CCTB, Late Carboniferous and Permian magmatic activities are recognized in the North Tianshan Belt, the South Tianshan Belt and the northern margin of Tarim Craton as well. In the NTB, the accretionary belt north of the YB and CCTB, Late Carboniferous to Early Permian (~303 to ~288 Ma) autocrystic zircons from A-type granites exclusively have positive zircon εHf(t) values from +2.79 to +14.10 with T_{DM}^{C} from 0.42 to 1.14 Ga (Fig. 7e). In the STB, Late Carboniferous to Middle Permian felsic rocks display negative to slightly positive εHf(t) (*t* ranges from ~316 to ~264 Ma) values (−9.97 to +4.21) and relatively ancient crustal Hf model ages (1.03–1.93 Ga). The Permian (~291 to ~269 Ma) alkaline (A-type) granites exposed in the western part of the NTC are characterized by comparatively juvenile Hf isotopic features, as suggested by εHf(t) of −0.80 to +16.12 and T_{DM}^{C} of 0.28–1.36 Ga (Figs. 4a and 7e).

6. Temporal Spatial and Nd-isotope variations in the Yili Block and adjacent regions

Nd isotopic analysis was not carried out by the present study, and

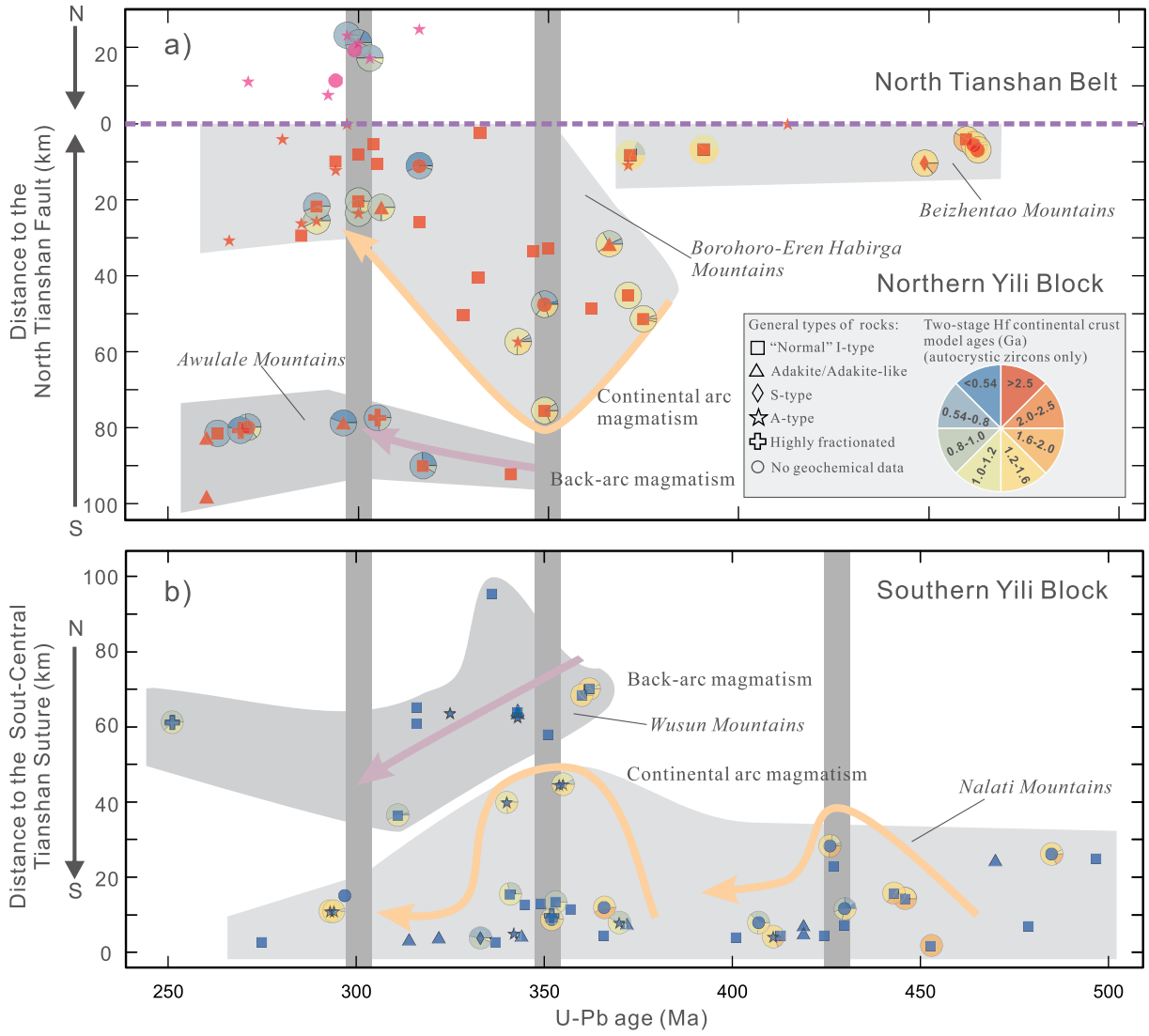

Fig. 6. U-Pb rock age versus distance to the suture of Paleozoic granitoid intrusions and felsic volcanic suites in the (a) northern and (b) southern parts of the Yili Block, showing development and migration of continental arc and back-arc magmatism. Relative abundances of T_{DM}^{C} for autocrystic zircon grains and general rock types of each intrusion/volcanic suite are displayed in the figure. Data used for plots are listed in Table S2.1 in Supplementary Material 2.

results were compiled from the literature. A total of 166 sets of whole-rock Nd isotopic results from 60 Paleozoic felsic plutons/volcanic suites were compiled, and the results are listed in Table S2.3 in Supplementary Material 2. The location and average value of two-stage Nd model ages (T_{DM2}) for each of plutons/volcanic suites are illustrated in Fig. 9a. Compared with Hf isotope, Nd isotope analyses have been conducted for a smaller number of plutons/volcanic suites of the West Tianshan, and the available data are spatially concentrated in the Yili Block (Fig. 9a). For the western part of the YB, a T_{DM2} contour map (Fig. 9b) was produced in ArcGIS using the inverse distance weighted interpolation method, based on the average values of T_{DM2} for individual plutons/volcanic suites.

A small number of Nd isotopic results were reported for Early Paleozoic (~479 to ~401 Ma) felsic rocks in the southern YB. The εNd (t) values range from −6.85 to +1.38, and T_{DM2} from 1.05 to 1.75 Ga (Fig. 10). In the South Tianshan Belt, samples from a ~423 Ma granitic pluton possess εNd(t) of −7.33 to −3.72 and corresponding T_{DM2} of 1.47–1.77 Ga (Fig. 10).

Late Devonian to Early Carboniferous felsic rocks from the northern YB (with ages from ~371 to ~346 Ma) have a wide range of εNd(t) (−5.63 to +2.94) and T_{DM2} (0.87–1.58 Ga), and the Late Carboniferous ones (with ages from ~317 to ~306 Ma) show comparatively depleted Nd isotopic signatures [εNd(t) = −0.11 to +3.34 and T_{DM2} = 0.81–1.09 Ga] (Fig. 10). In the southern YB, a few Nd isotopic data were reported from Late Devonian to Late Carboniferous felsic rocks (with ages of ~362 to ~316 Ma). The εNd(t) values vary from −3.51 to +4.48 and T_{DM2} from 0.73 to 1.41 Ga. As shown in Fig. 10, felsic rocks from both northern and southern parts of YB possess a Nd isotopic pull-up to more juvenile characteristics with decreasing age during the Late Devonian to Late Carboniferous, similar to the tendency exhibited by Hf isotopic results (Fig. 7b and c).

In the northern YB, felsic rocks formed during the Permian show juvenile to slightly evolved Nd isotopic signatures with εNd(t) of −1.73 to +3.42 (*t* ranges from 260 to 296 Ma) and T_{DM2} = 0.76–1.20 Ga (Fig. 10). By contrast, a few Early Permian granitoids from the southern YB display more evolved Nd isotopic features, as suggested by εNd(t) varying from −6.00 to −0.51 (*t* ranges from 275 to 294 Ma) and T_{DM2} from 1.02 to 1.63 Ga (Fig. 10).

In terms of Nd isotope, the most "juvenile" granites were recognized in the Late Carboniferous to Early Permian A-type granites from the North Tianshan Belt [εNd(t) = +2.96 to +7.35, *t* varies from ~315 to ~298 Ma; T_{DM2} = 0.47–0.83 Ga] (Figs. 9a and 10). On the contrary, the most Nd isotopically "ancient" Late Carboniferous to Early Permian felsic rocks can be recognized in the South Tianshan Belt, as they have

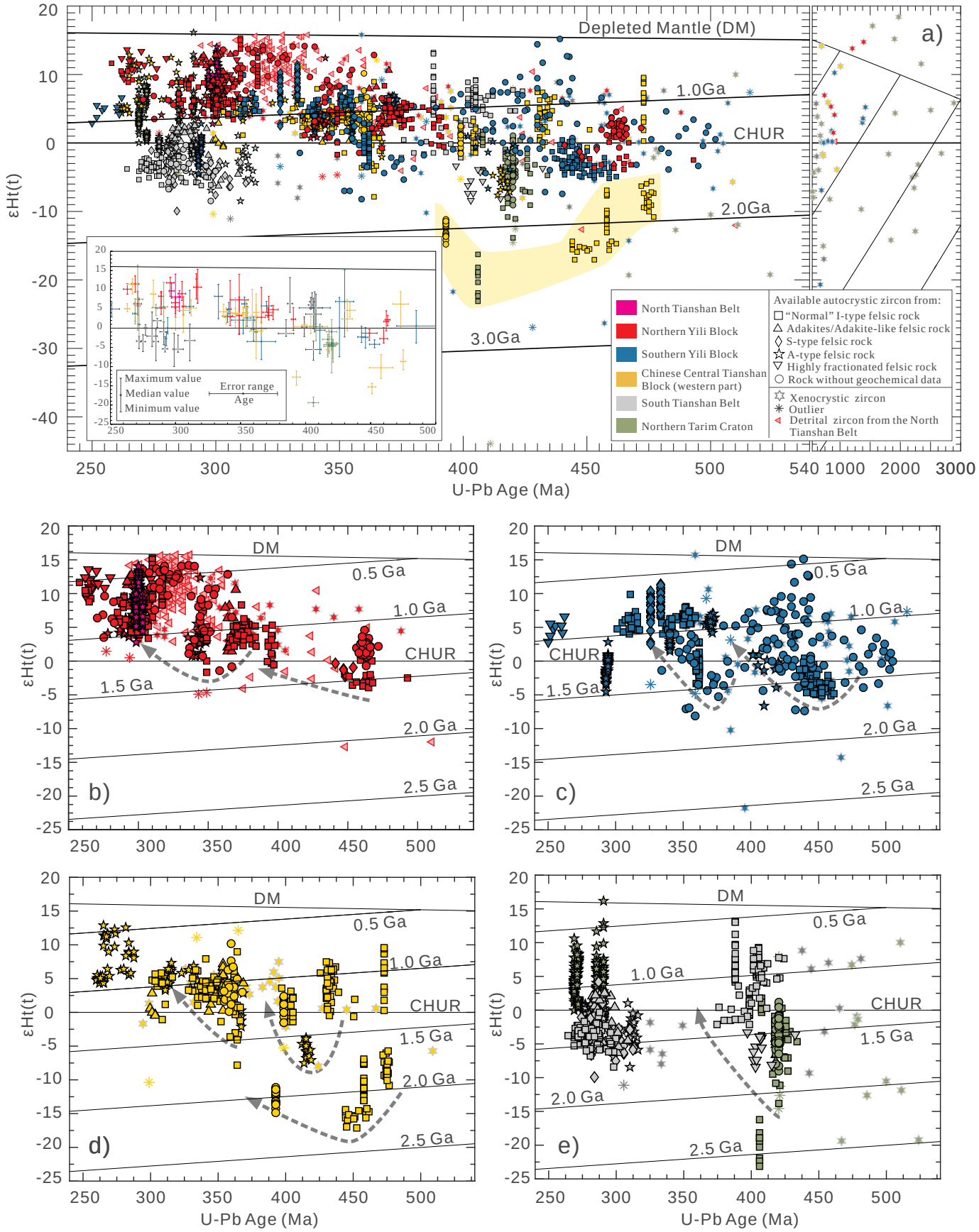

Fig. 7. Plot of εHf(t) values vs. U-Pb ages of zircons from Paleozoic granitoid intrusions and felsic volcanic suites in the West Tianshan. Calculation of model ages (T_{DM}^{C}) and notations of chondritic uniform reservoir (CHUR) and depleted mantle (DM) curves are given in the figure. Data are from this study and literature (see data for felsic rocks in Table S2.2 in Supplementary Material 2, and data for detrital zircons from the North Tianshan Belt in Wang et al., 2018b).

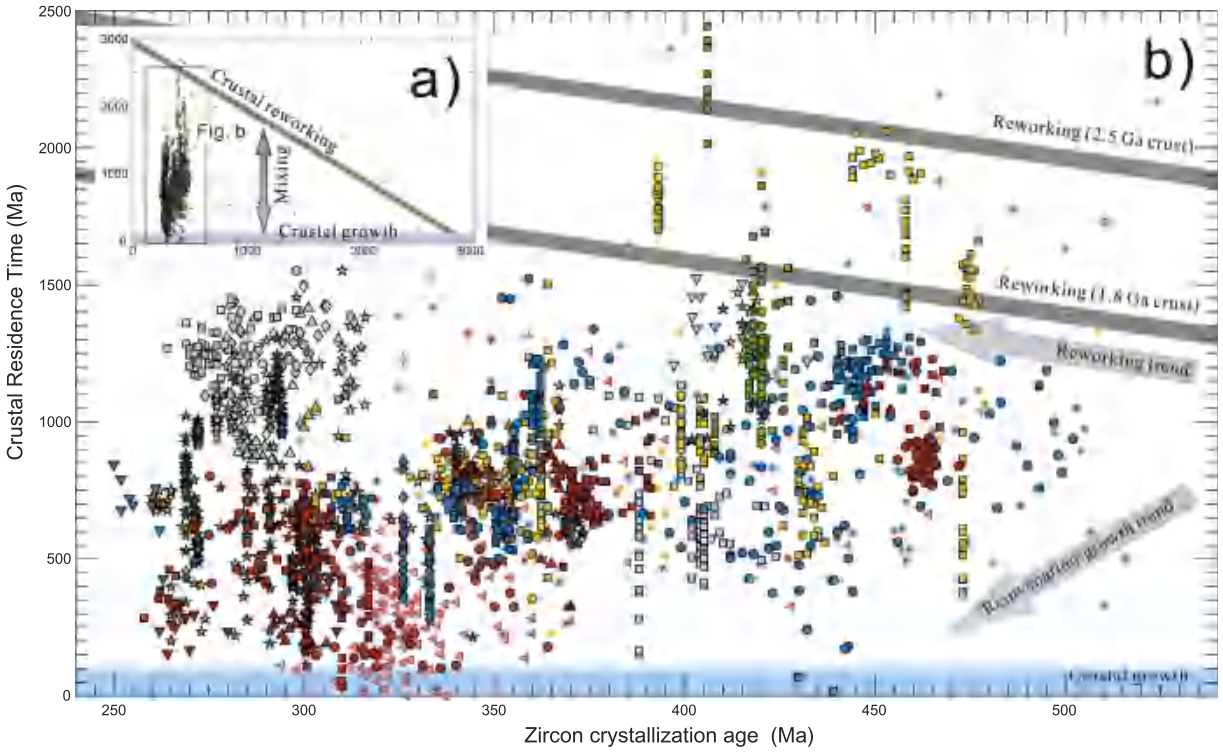

Fig. 8. Plot of crustal residence time vs. crystallization ages of the Paleozoic felsic rocks from the West Tianshan, showing the relationship of the magmatic events and crustal evolutions. The crustal residence time is the interval between the crustal Hf model age and the crystallization ($^{206}Pb/^{238}U$) age of the zircon. In this plot, an upward trend with decreasing age implies reworking of the pre-existing crust, while a horizontal or downward trend implies continental growth by juvenile input. Symbols and data sources are as in Fig. 7.

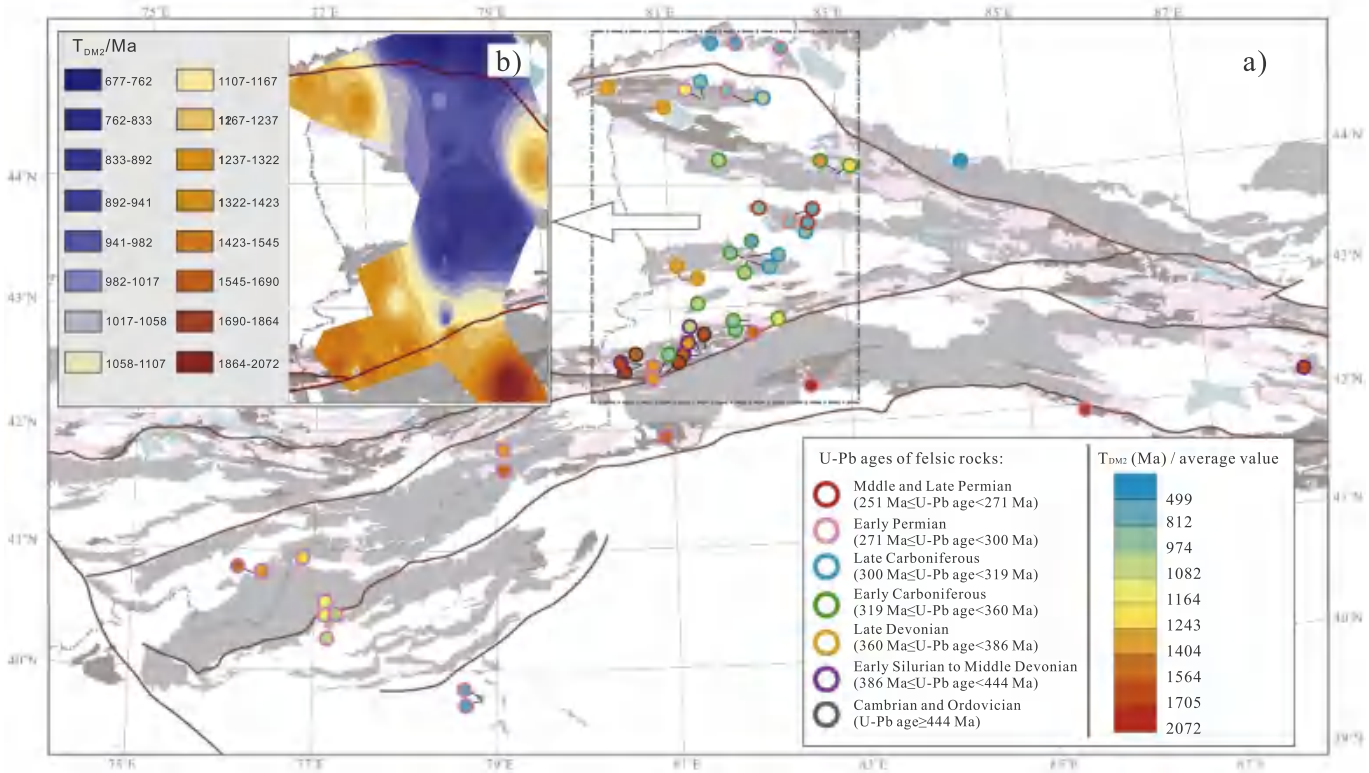

Fig. 9. (a) Map of two-stage Nd model ages (T_{DM2}) for felsic rocks of the West Tianshan, showing average value of T_{DM2} for each pluton/volcanic suite; (b) Nd isotope contour map showing the spatial variation of T_{DM2} for each pluton/volcanic suite. Data used for Nd isotopic mapping are listed in Table S2.3 in Supplementary Material 2.

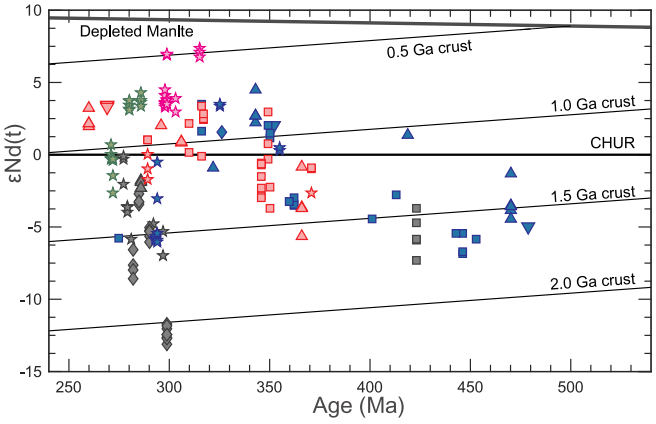

Fig. 10. Plot of whole-rock εNd(t) values vs. crystallization age for the Paleozoic felsic intrusions/volcanic suites from the West Tianshan. Symbols are as in Fig. 3. Data used for plot are listed in Table S2.3 in Supplementary Material 2.

variable and consistently negative εNd(t) values (−13.09 to −0.10, *t* ranges from 277 to 299 Ma) and ancient T_{DM2} (1.00–2.12 Ga) (Figs. 9a and 10). In the northern Tarim Craton, the Permian alkaline (A-type) granites and syenites exposed possess εNd(t) of −2.61 to +4.30 (*t* ranges from 286 to 271 Ma) and T_{DM2} of 0.61–1.15 Ga (Fig. 10).

As illustrated in Fig. 11, a comparison between average εNd(t) and median εHf(t) values for individual plutons/volcanic suites indicates generally coupled Nd–Hf isotopic features of the Paleozoic felsic rocks in the West Tianshan. Except for two outliners, regression through these data yield an array of y = 1.3423x + 4.9759 with a similar slope to that of the proposed terrestrial array (y = 1.36x + 2.95) (Vervoort et al., 1999) despite a small y-axis offset. The two outliners are garnet-bearing S-type granitic pluton (SY33)/rhyolitic lava flow (SY43) both from the peraluminous magmatic belt in the southern South Tianshan Belt (see details below), which implies that the involvement of garnet in magma genesis ("garnet effect", Ionov et al., 2005; Schmidberger et al., 2002; Huang et al., 2017b) and/or recycling of sedimentary materials in the magma source ("zircon effect", Patchett et al., 1984) might account for Nd-Hf isotope decoupling. Besides, it is worth noting that the two-stage Nd model age contour map (Fig. 10b) shows a distinct space-dependent pattern of the Yili Block, which is comparable to that shown in the crustal Hf model age contour map (Fig. 5). In summary, in the West Tianshan, particularly Yili Block, the inferences regarding continental crustal growth/reworking and distribution of juvenile, mixed and ancient crusts obtained from Hf isotopic signatures, as discussed later, can be supported by Nd isotope as well, given the similarity of the two isotopic systems in space and time.

7. Discussion

7.1. Tectonic division of the West Tianshan

As mentioned above, there are different division schemes of the West Tianshan. Some researchers suggested that the Nikolaev Line in Kyrgyzstan (the major fault with no. 4 in Fig. 1c), the northern border of the Kyrgyz Middle Tianshan Block, continues eastward into China and join the North Nalati Fault (the major fault with no. 6 in Fig. 1c), and thus regarded that the KMTB could be connected to the Chinese Central Tianshan Block through the southernmost margin of the "Yili Block" referred to in this study (e.g., Gao et al., 2009; Qian et al., 2007). However, the strata of the KMTB mainly developed on a passive continental margin and are dominated by middle Devonian to upper Carboniferous shallow-marine siliciclastic and carbonate deposits (Konopelko et al., 2008; Biske and Seltmann, 2010), and are overprinted by rare Carboniferous to early Permian intrusions and volcanic rocks (Alekseev et al., 2009). Contrary to this, Paleozoic igneous rocks are widely distributed on the southern margin of the YB, but Devonian sedimentation is lacking (Xia et al., 2014; Cao et al., 2017). Such geologic features of the YB are more comparable to that of the Kyrgyz North Tianshan (Chen et al., 1999a; Biske and Seltmann, 2010).

Regarding the nature of the Precambrian basement in the YB and CCTB, in-situ basement rocks older than Mesoproterozoic are well exposed in the CCTB, but have not yet been found in the Yili Block (Wang et al., 2017; Huang et al., 2019b). The absence of autocrystic zircons with T_{DM}^{C} > 1.8 Ga in the YB and comparative abundance of ones with Paleo-proterozoic T_{DM}^{C} in the CCTB might also reflect this difference (Figs. 4a and 7a, see below). Therefore, these observations do not support the speculation that regards the southernmost margin of the YB as a part of the CCTB.

Taking the facts mentioned above into account, we follow the consideration that the Nikolaev line terminate close to the China-Kyrgyzstan border (Biske and Seltmann, 2010), and the CCTB should not be connected to the KMTB.

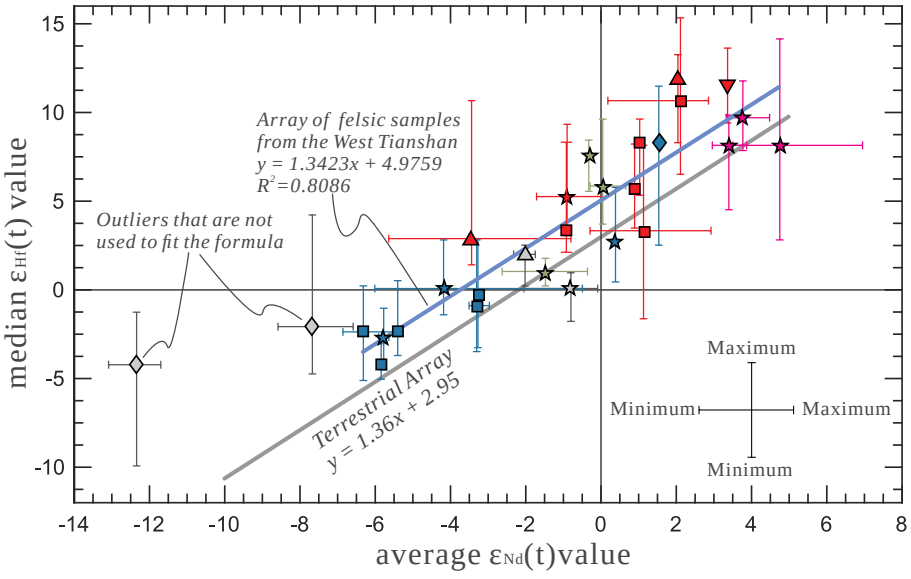

Fig. 11. Diagram of average εNd(t) value vs. median εHf(t) value of individual Paleozoic granitoid intrusions and felsic volcanic suites in some areas of the West Tianshan. Zircon εHf(t) values are coupled with εNd(t) for most intrusions/volcanic suites with few exceptions. See Supplementary Material 2 for details. Reference Terrestrial Array (εHf = 1.36εNd + 2.95) after Vervoort et al. (1999). Symbols are as in Fig. 3.

7.2. Implications for the crustal evolution

When radiogenic isotope data at a terrane-scale are used to address scientific issues, such as long-term tectonic evolution, the architecture of deep lithosphere, and continental growth and recycling, a haunting question arises as to where the spatial and temporal variations of isotopic signatures come. For instance, in previous studies carried out in Phanerozoic accretionary orogens (e.g., Cordillera, Andes and CAOB), the spatial heterogeneity in Nd-Hf isotope of Phanerozoic felsic rocks were explained by isotopic heterogeneity of the Precambrian basement (Chapman et al., 2018), and different degrees of mixing between syn-accretionary juvenile (newly formed) components and pre-accretionary old basement rocks (Hou et al., 2015; Zhang et al., 2019b; Song et al., 2019). Identifying the primary control that leads to isotopic diversity in space and time is a top priority before using the compiled dataset to address any scientific issues.

The synthesis of the Hf-in-zircon isotopic dataset of Paleozoic felsic rocks in the Yili Block and adjacent regions reveal remarkable spatial and temporal heterogeneity for their sources as well. In Western Tianshan, the oldest crustal components involved in the Paleozoic felsic magmatism is recorded by autocrystic zircons with > 1.8 Ga T_{DM}^{C} (Figs. 4a, 7d and f), hosted by felsic rocks from the southern margin of the western CCTB and by ones from the Kuruktag area of the NTC (e.g., nos. T05, and CT03, 04, 09 and 33 in Fig. 4a). Regarding to the Yili Block, however, despite few Precambrian to earliest Cambrian zircon xenocrysts with older T_{DM}^{C} from felsic rocks of the southern YB, zircons with T_{DM}^{C} > 1.8 Ga are absent in the whole YB (Fig. 7b and c), implying that Paleoproterozoic and older basement rarely existed beneath the YB when the micro-continent was being involved in the Phanerozoic CAOB evolution. These ancient crustal sources might have been involved and exhausted in the Precambrian tectonomagmatic events. For instance, Neoproterozoic (~920 to ~845 Ma) granitic rocks of the Wenquan metamorphic complex display whole-rock two-stage Nd model ages from ~2.14 to ~1.51 Ga (Wang et al., 2014a, 2014b). Filtering out those with T_{DM}^{C} > 1.8 Ga, zircons with crystallization ages > 320 Ma from different tectonic units of the Western Tianshan, in particular from Yili and Central Tianshan blocks, display comparable trends on εHf(t)-age and crustal residence time-age (Hf) plots (Figs. 7a and 8), regardless of differences in the range of absolute values at any specific period. Such a similarity implies that changes of involvement of newly added juvenile material in magma sources exert primary control on the terrane-scale secular change of zircon Hf isotopic composition, and that the degrees of involvement of juvenile material were likely associated with the changing tectonic regimes of the SW CAOB.

The above inference is further corroborated by spatial Hf-isotope variation of the Yili Block. For deep crustal rocks of cratons or micro-continents, a general trend from ancient components in the inner part to relatively juvenile components towards the margin is expected. Besides, during the oceanic subduction, more amounts of mantle materials are expected to participate in the arc-type magmatism towards the trench. Therefore, in most margins of cratons or micro-continents being subducted, a 'normal' spatial isotopic trend of arc-type felsic rocks is most isotopically juvenile near the trench and becomes increasingly evolved landward, such as illustrated by felsic rocks from southern U.S. Cordillera and Lhasa Terrane in Southern Tibet (e.g., Bowring and Karlstrom, 1990; Wooden et al., 2013; Zhu et al., 2011; Hou et al., 2015; Chapman et al., 2017). However, the spatial variation in Hf-zircon isotope for felsic rocks from the Yili Block shows that relative ancient basement rocks intersperse in its northern and southern edges, and the most juvenile crust is recorded beneath its centre. Geophysically, the Hf isotopic juvenile domains of the Yili Block coincide spatially with high magnetic anomalies (Fig. 4b), implying more mafic crustal compositions underlying these domains. Since no any suture has been recognized in the central part of the Yili Block (Yili Basin) to date, the above facts together suggest that the ancient basement of the YB had been partially replaced by juvenile crust, a process that might be reflected by long-term temporal trends in radiogenic isotopic data.

The present level of erosion is characterized by voluminous felsic intrusions and volcanic units and a relative scarcity of intermediate to basic magmatic rocks (Fig. 1c). Therefore, summarizing the changing proportions of juvenile components contributing to these Paleozoic felsic rocks in space and time might mirror the whole picture of the Phanerozoic continental growth and reworking. Reworking of ancient crust likely occurred in the Yili and Central Tianshan blocks during the Middle Cambrian to Late Ordovician, as suggested by downward trends for pre-Silurian (≥ca. 445 Ma) felsic magmatism of the two blocks and by the dominance of T_{DM}^{C} > 1.0 Ga whether in a single intrusion/volcanic suite or all samples (Fig. 7b, c and d). Subsequently, substantial crustal growth was recorded by rising trends in εHf values of autocrystic zircons aged between ~430 and ~390 Ma in the southern YB, between ~420 to ~400 Ma in the CCTB and between ~420 to ~385 Ma in the STB and NTC. A sudden decreasing trend was recorded by latest Devonian zircons (~375 to ~359 Ma) from the YB and CCTB, implying a period of ancient crust reworking (Fig. 7b, c and d). As suggested by Hf-in-zircon isotope ratios trended towards more radiogenic values and narrowed, significant input of juvenile material is likely an inherent feature of the Early Carboniferous (~359 to ~319 Ma) accretionary evolution in YB and CCTB (Fig. 7b, c and d). The Late Carboniferous to Late Permian crustal evolution in the Western Tianshan was spatially heterogeneous. In the South Tianshan Belt, the recommenced Permian magmatism likely record continental crustal evolution dominated by reworking of ancient basement rocks, and by contrast, that from the northern Tarim Craton and North Tianshan Belt suggest high-degree involvement of juvenile material s (Fig. 7e). On the plot of age versus crustal residence time (Fig. 8), Late Carboniferous to Late Permian autocrystic zircons from Yili and Chinese Central Tianshan blocks show roughly constant to slightly upward evolutionary trends, despite being dominated by ones with juvenile isotopic signatures. This implies that, as a whole, Late Carboniferous to Late Permian felsic magmatism occurring in these micro-continents mainly retain pre-existing isotopic signatures of crustal sources, and might record a period of upward transport and stabilization of juvenile components.

In summary, during most of the Paleozoic, felsic magmatism in the Yili Block and adjacent regions was characterized by episodic dominance of juvenile crustal components, implying that the CAOB accretionary orogenesis played an essential role in the formation and preferential preservation of juvenile crust. Consequently, the main question then arises, that is, when and how did such a "rejuvenation" process occur?

7.3. Periodic trench advance and retreat

The Paleozoic tectono-magmatic events in the Yili Block and adjacent regions were associated with the subduction of branches of the SW Paleo-Asian Ocean and the following orogenic collage. There existed two main oceanic branches, i.e., the South Tianshan Ocean in the south and the North Tianshan Ocean (southern section of the Junggar Ocean) in the north (Long et al., 2011; Xiao et al., 2013; Han and Zhao, 2018; Gao et al., 2018). Besides, an oceanic basin, which is termed as Central Tianshan Ocean or Turskey Ocean, existed between the YB and Central Tianshan Block during Early Paleozoic times and (Qian et al., 2007; Gao et al., 2009; Han et al., 2015). The origin of the South Tianshan Ocean remains debated; the proposed models include the Early Paleozoic opening initiated as a back-arc basin of North Tianshan Ocean and/or Central Tianshan Ocean (Han et al., 2015; Long et al., 2011; Wang et al., 2011, and references therein), and the Late Neoproterozoic opening model resulted from the rifting processes in the northern Tarim Craton (e.g., Ge et al., 2012b, 2014; Huang et al., 2013, 2019a). According to published data sets (Jiang et al., 2014; Han and Zhao, 2018, and reference therein; Hegner et al., 2019), the mafic-ultramafic rocks within ophiolites exposed in the South Tianshan Belt

mainly have Late Ordovician to Middle Devonian crystallization ages, and exhibit geochemical signatures indicating a suprasubduction zone (SSZ) origin. Therefore, regardless of the origin of the South Tianshan Ocean, the subduction of this oceanic slab should have begun earlier than the formation of most Early Paleozoic magmatic rocks exposed in Chinese Western Tianshan. On the other hand, the closure of the Central Tianshan Ocean, inducing the amalgamation of the Yili and Central Tianshan blocks, likely took place no later than the Early Devonian (Bazhenov et al., 2003; Burtman, 2008; Konopelko et al., 2008; Qian et al., 2009; Gao et al., 2009; Wilhem et al., 2012). Since the CCTB is unlikely connected to the Kyrgyz Middle Tianshan Block, as discussed above, the role of subduction of the Central Tianshan Ocean in the Early Paleozoic tectono-magmatism of the Chinese Western Tianshan seems insignificant.

In summary, subduction and closure of the South Tianshan Ocean in the south and the North Tianshan Ocean in the north played a major role in the genesis of Paleozoic igneous rocks. In the current study, we consider that the final closure of the South Tianshan Ocean likely took place during the Late Carboniferous, and the south-dipping subduction beneath the northern YB might terminate at the end of the Carboniferous (see details below). As illustrated in the histogram (Fig. 2b), pre-latest Carboniferous ages for felsic rocks from the YB yield two major populations of ~460 to ~395 Ma and ~375 to ~310 Ma, respectively, implying two epochs of subduction events separated by a magmatic lull (Fig. 12a and b). This interpretation is reinforced by several detrital zircon geochronological data sets (e.g., Ren et al., 2011; Liu et al., 2013; Huang et al., 2018; Huang et al., 2019a).

During the first stage, a double-sided subduction event of the South Tianshan Ocean is inferred from the synchronical magmatic record in the southern YB and the STB-NTC (Fig. 12a; Ge et al., 2012b; Jiang et al., 2014; Huang et al., 2019a). During the second stage, the northern Tarim margin was likely a passive margin (Fig. 12b) since no Late Devonian and Early Carboniferous continental arc-type magmatism has been recognized so far. Given the widespread occurrence of ~ 375 to ~320 Ma continental arc-type rocks in the southern YB (Fig. 2; Zhu et al., 2009), northward subduction of the South Tianshan Ocean during Late Devonian and Early Carboniferous is more likely. Besides, the compiled geochronological data suggest that the continental arc magmatism developed on the northern margin of the YB since as early as the Late Ordovician (Fig. 12d; ~460 Ma).

An inherent feature of the long-term evolution of accretionary orogens is the periodic occurrence of trench advance and retreat (Aitchison and Buckman, 2012). A tectonic switch from advancing- to retreating-type accretion could be triggered by the slab rollback that results from the gravity and/or a thickened overlying continental lithosphere (Antonijevic et al., 2015; Niu, 2018; Ji et al., 2019). When the oceanic crust was deep enough to undergo sufficient eclogitization to become negatively buoyant, the subducting slab tends to rotate vertically, finally leading to slab rollback. The intermittent arrival of buoyant oceanic plateaus likely induces flat subduction (Collins, 2002; Gazel et al., 2015; Hao et al., 2018), which could result in the disappearance of the asthenospheric wedge (Gutscher et al., 2000; Hao et al., 2018) and waning or ending of arc magmatism (Axen et al., 2018). Low- to normal-angle subduction re-commences once the major part of the arrived oceanic plateau is subducted, possibly resulting in a transient period of trench advance followed by slab rollback (Kemp et al., 2009; Collins et al., 2019). Concerning the continental growth, in some well-studied orogens or present-day continental margins, e.g., the Tasmanides of eastern Australia (Kemp et al., 2009; Phillips et al., 2011; Collins et al., 2019), Andes (Boekhout et al., 2015; del Rey et al., 2016), Neo-Tethyan arc system from southern Tibet to Sumatra (Zhang et al., 2019a), long-term continental growth in the upper plate was attributed to magma formation during retreating subduction related to slab rollback, although other mechanisms, such as lithosphere delamination, slab break-off and mantle plume(s), might play a subordinated role. On the contrary, subduction advance plausibly caused the closure of intra- or back-arc basins and increased crustal thickness, and thereby lead to greater involvement of reworked, ancient crustal material (Kay et al., 2005; Boekhout et al., 2015). As aforementioned, the Hf-in-zircon isotopic mapping of felsic rocks from the YB and CCTB record alternating crustal growth and reworking, and, therefore, the periodic tectonic transition is also preferred for the accretionary history of these microcontinents.

Although isotopic and geochemical data for > 420 Ma rocks are limited, significant inputs of juvenile materials were recorded by rising trends in εHf values of ~430 and ~390 Ma autocrystic zircons in the southern YB and ~420 to ~385 Ma ones in the STB. This, coupled with the decrease in Sr/Yb and Sr/Y with decreasing age presented in ~420 to ~400 Ma felsic rocks in the southern YB and ~420 to ~385 Ma ones in the STB and northern Tarim Craton (Fig. 3d and h), implies the increasing proportion of juvenile contributions and the shallowing of melting depths. These observations are best explained by a tectonic switch from an early episode of compression and crustal thickening due to advancing-type accretion (Fig. 12e), to a later extension and crustal thinning due to retreating-type accretion (Fig. 12f), possibly coupled with other mechanisms such as slab break off and lithosphere delamination (Zhang et al., 2019b). Reinforcing this view is the abundance of fold-thrust structures in Ordovician strata but absence in Silurian strata in the northern Tarim Craton (Li et al., 2015b; Zhang et al., 2019b). Given the E-MORB-like gabbros recently identified in the southern STB (e.g., Zhao et al., 2015), a western Pacific-type trench-arc-back-arc basin system was at least developed at the northern edge of the Paleozoic Tarim resulting from the northward retreat of the southward-dipping subduction zone (Fig. 12f).

In terms of the first-stage evolution of North Tianshan Ocean in the Chinese Western Tianshan, to get a convincing description is hindered due to the insufficient data. However, based on previous studies carried out in the Chinese Eastern Tianshan, such as the analysis of Hf isotopic trends of Early Paleozoic detrital and magmatic zircons from the Chinese Eastern Tianshan (e.g., Zhang et al., 2016a, 2016b, 2019b), slab rollback/retreat of the North Tianshan Ocean probably occurred since ca. 450–440 Ma, and we tentatively follow this line of thinking (Fig. 12e).

Some intrusive rocks formed in the early-stage subduction in the West Tianshan were ductilely deformed and metamorphosed to upper-greenschist to amphibolite facies, whereas ones related to the late-stage subduction were undeformed and unmetamorphosed (Gao et al., 2009; Zhong et al., 2017; Cao et al., 2017). This difference implies that an episode of contractional deformation plausibly accompanied the ~20 My (~395 Ma to ~375 Ma) magmatic quiescence. As mentioned, the arrival of buoyant oceanic plateaus is a likely mechanism that leads to the flat subduction, tectonic switch from extension to contraction, and waning of the arc magmatism. In the SW CAOB, Early Paleozoic OIB-type alkaline basalts have been recognized in several ophiolitic mélanges, such as Heiyingshan ophiolitic mélange complex in the South Tianshan Belt, Darbut and Karamay ophiolitic mélanges in the West Junggar (Wang et al., 2011; Yang et al., 2015, 2018a, 2018b, 2019, and references therein). They were considered as accreted seamount fragments and may represent mantle plume-related magmatism within the Paleozoic-Asian Ocean. We tentatively propose that the arrival and subduction of some large-volume seamounts at ~390 Ma might account for the transient magmatic lull (Fig. 12g). There still exist other possibilities regarding the potential components of the accreted oceanic plateaus, and further studies are needed.

Late Paleozoic arc-back-arc systems are recognizable in the Yili Block. In the southern YB, some previous studies have unveiled the development of a back-arc basin in the Wusun Mountain and nearby areas (e.g., Cao et al., 2017; Su et al., 2018; Wang et al., 2018e, 2020). The back-arc magmatism is plausibly represented by Lower Carboniferous Dahalajunshan Formation (Fm.) consisting of felsic-intermediate marine volcanic rocks (e.g., SY50 in Fig. 2a), overlying Lower Carboniferous Akeshake Fm. comprising a suite of marine limestone and

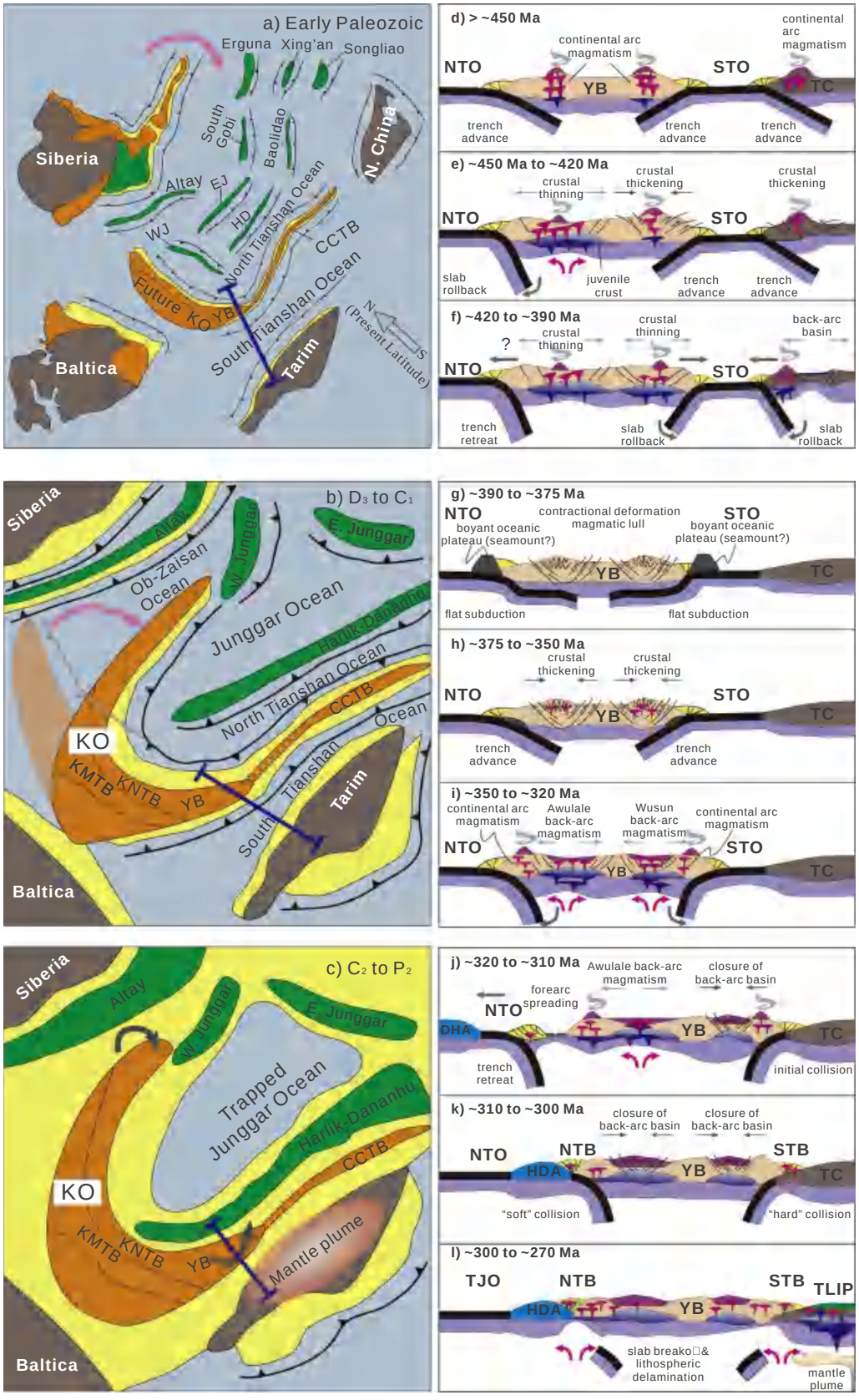

Fig. 12. Geodynamic model and palaeogeographical reconstruction for Palaeozoic evolution of the SW part of the Palaeo-Asian Ocean. Palaeogeographical reconstruction is modified after Windley et al. (2007), Xiao et al. (2010), Wilde (2015) and Gao et al. (2018). See text for more details.

Abbreviations: NTO-North Tianshan Ocean; STO-South Tianshan Ocean; TC-Tarim Craton; YB-Yili Block; CCTB-Chinese Central Tianshan Block; KNTB-Kyrgyz North Tianshan Block; KMTB-Kyrgyz Middle Tianshan Block; KO- Kazakhstan Orocline; STB-South Tianshan Belt; NTB-North Tianshan Belt; HDA-Harlik-Dananhu arc; TLIP-Tarim Large Igneous Province; TJO-Trapped Junggar Ocean

terrigenous clastic rocks (Li et al., 2017), and slightly younger gabbros and granitoids (nos. SY18, 19, 20, 53 in Fig. 2a) intruding the aforementioned volcano-sedimentary successions (Cao et al., 2017; Su et al., 2018; Wang et al., 2018f, 2020). There is no evidence for the existence of back-arc oceanic crust in the Wusun Mountain and nearby areas, which leads us to interpret it as an immature back-arc basin.

In the northern YB, voluminous mafic volcanic rocks (e.g., basalt, trachy-basalt, trachy-andesite), formed during ca. 320–310 Ma and

genetically related to some large- and super-large-scale submarine volcanic-hosted iron deposits, are preserved in the Awulale Mountains (Ge et al., 2015; Yan et al., 2015). Geochemical and isotopic compositions of these mafic volcanic rocks and plutonic counterparts suggest that their parental magmas were mainly derived from high-degree partial melting of subduction-related modified mantle sources in the spinel stability field with the involvement of deep MORB-like components (Yan et al., 2015; Wang et al., 2018c). A Late Carboniferous nascent back-arc system was likely developed in the northern YB, and the Awulale Mountains acted as a back-arc rifting centre.

Therefore, in terms of the Late Paleozoic subduction-related magmatism, rocks preserved in Borohoro-Eren Habirga Mountains in the northern YB and Nalati Mountains in the southern YB were parts of Paleozoic continental arcs, whereas ones in Awulale Mountains in the north and Wusun Mountains in the south are products of back-arc magmatism. As shown in Fig. 6, for felsic rocks in the Nalati Mountains in the southern YB, the longest distance between compiled rocks and the suture increases during ~370 to ~350 Ma and decreases during ~350 to ~322 Ma; for ones from Borohoro-Eren Habirga Mountains, a transition from increase to decrease likely took place around ~350 Ma as well. Such spatial and temporary variations likely record alternating landward and oceanward arc magmatic migration resulting from periodic trench advance and retreat (Fig. 12h and i).

Recent P-T-deformation-time and kinematic constraints for metamorphic rocks in the HP-UHP metamorphic complex along the South Tianshan Suture indicate the change in slab geometry of the South Tianshan Ocean (Tan et al., 2019). The diachronous recovery of different sub-units, from ~45 km (metamorphosed meta-mafic/-ultramafic unit; ~360 Ma), ~65 km (eclogite/blueschist facies unit; ~330 Ma) and ~85 km depth (UH unit; ~320 Ma) is consistent with a transient (latest Devonian and earliest Carboniferous) low-angle subduction followed by long-term steepening of the subducted plate (slab rollback). The transition from advancing to retreating subduction is also supported by secular elemental and isotopic trends of the felsic rocks. A sudden decreasing trend in εHf(t) values presented in latest Devonian zircons (~375 to ~359 Ma) and an increasing trend in Sr/Y and Sr/Yb ratios in ~375 to ~350 Ma felsic rocks from the southern YB likely reflect the thickening of regional crust. Subsequently, downward trends in these ratios presented by ~350 to ~322 Ma felsic rocks imply that the onset of crustal extension and thinning due to trench retreat plausibly occurred in the earliest Carboniferous (Fig. 12i).

In the northern YB, aside from the migration of continental arc magmatism, a tectonic switch from trench advance to retreat in the second-stage subduction of the North Tianshan Ocean is also in agreement with the compiled elemental and isotopic data. The secular tendency in Sr/Y and Sr/Yb in felsic rocks changed from rough increasing trends before ~366 Ma to rough decreasing trends after ~366 Ma (Fig. 3a and e), and the shift of the evolutionary trend in εHf(t) from decrease to increase occurred at ~350 Ma (Fig. 7b). The Carboniferous retreat subduction might result in the decompression melting of the upwelling asthenosphere in a forearc setting, as recorded by N-MORB-, E-MORB- and OIB-like mafic rocks within ophiolitic fragments in the North Tianshan Belt (Li et al., 2015a; Feng and Zhu, 2018) (Fig. 12J). The steeply dipping subducting slab beneath the northern YB still existed in the Late Carboniferous, as suggested by the recognition of Late Carboniferous sodium-rich adakites and Nb-enriched arc basalts in the Alataw area in the North Tianshan Belt (Wang et al., 2007b) (Fig. 12j).

In summary, the compiled dataset of felsic rocks from the YB, coupled with other evidence, is capable of unveiling periodic trench advance and retreat during the two epochs of subduction. In the first-stage subduction, tectonic switch of the North Tianshan Ocean from advancing to retreating subduction took place around ~450 Ma and that of the South Tianshan Ocean around ~420 Ma. The second-stage subduction was characterized by a period of trench advance (~ 375 to ~350 Ma of the North Tianshan Ocean and ~370 to ~350 Ma of the South Tianshan Ocean) at the initiation and the following Early Carboniferous trench retreat (~350 to ~310 Ma of the North Tianshan Ocean, and ~350 to ~322 Ma of the South Tianshan Ocean) associated with the development of back-arc basins. Note that the above-summarized alternating trench advance and retreat might be recorded in the western Chinese Central Tianshan Block as well, since 1) pre-Late Carboniferous granitoids in western CCTB show comparable secular elemental and Hf isotopic variations and 2) the pre-Early Devonian amalgamation of the two micro-continents, as mentioned above. However, distinguishing between North Tianshan Ocean-related and South Tianshan Ocean related arc-back-arc systems in the CCTB is difficult, due to its narrow north-south width.

In the YB and CCTB, with few exceptions, pronounced variability in Hf isotope are presented within individual samples at the beginning of each period of trench retreat; then variations gradually decrease with decreasing age, and relatively muted variations can be observed at the end of the period (Fig. 6a and b). Such a scenario further argues for the crucial link between subduction and continental growth. During an episode of retreat subduction, with time, basaltic, isotopically juvenile magmatic additions at the base of crust may impart the juvenile isotopic composition on the lower crust, and give rise to a more juvenile and homogenous deep crust (Chapman et al., 2017). This process can be refected by diminishing ancient crustal components and long-termed homogenization for felsic magma sources.

7.4. Implications for assembly of the Western Tianshan orogenic collage

The time of closure of South Tianshan Ocean, which resulted in the amalgamation of Tarim Craton with the SW CAOB, is still debated (see Han et al., 2011; Gao et al., 2011; Xiao et al., 2013; Han and Zhao, 2018, and references therein). We prefer a Late Carboniferous collision (Fig. 12j and k). Multidisciplinary evidence (e.g., ages and distributions of ophiolites/ophiolitic mélanges, A-type granitoids, (U)HP metamorphic rocks, large-scale shear zones, and molasses) supporting this view has been reported and reviewed in many recent publications (e.g., Han et al., 2011; Gao et al., 2011; Han and Zhao, 2018; and references in these papers; Tan et al., 2019), and, therefore, we do not intend to discuss the issue from every aspect but emphasize that the Late Carboniferous collision model is in agreement with the spatial distribution and isotopic-geochemical signatures of Late Carboniferous and Permian felsic rocks from the southern Yili Block and South Tianshan Belt.

The CAOB includes predominantly accretionary (Pacific-type) orogens, but collisional (Himalayan-type) orogens can also be recognized (Safonova, 2017). Isotopically, felsic rocks emplaced during the latest Carboniferous to Early Permian in the South Tianshan Belt exhibit relatively more “ancient” Nd-Hf isotopic compositions than most of those coevally formed in the northern YB and CCTB (Fig. 7), and some of granitoids in STB finally intruded the country rocks carrying ophiolitic components (stitching granitic plutons, Han et al., 2011, and references therein), implying that their emplacement post-dated the collisional event during which the ophiolitic mélanges were obducted onto the arriving northern Tarim margin (Konopelko et al., 2007, 2009; Han et al., 2011). The dominance of recycled ancient crustal sources for post-accretionary felsic magmatism of the STB generally denotes an amalgamation ended with a “hard” continent-continent collision (i.e., a collisional orogenic belt) between the northern Tarim Craton and the southern limb of Kazakhstan composite continent (i.e., Kyrgyz Middle Tianshan, Yili and Chinese Middle Tianshan blocks). Such a hard collision might cause the cease of back-arc rifting within the Yili Block. Some adakite-like, intermediate-felsic intrusions (e.g., NY25, 26 and 27 in Fig. 2a) were emplaced during ~296 to ~260 Ma in the Awulale mountains of the northern YB (Zhao et al., 2008; Tang et al., 2017b). Recent studies suggest that the adakitic magmas were derived from the melting of the thickened mafic lower crust, induced by convective removal of the collision-thickened lithosphere (Tang et al., 2017b). Such an interpretation implies a back-arc closure and lithospheric thickening event before the Early Permian.

According to spatial distributions and geochemical compositions of Late Carboniferous to Early Permian magmatic rocks and other geologic evidence (e.g., Han et al., 2011; Gao et al., 2011; Han and Zhao, 2018; and references in these papers), magmatic responses in the southern YB and STB to the collisional event can be summarized as 1) minor normal I-type calc-alkaline and adakite-like granitoid magmatism (e.g., SY35, 36, 54 and 55 in Fig. 2a) emplaced in the early Late Carboniferous in the southern YB at the initial collision (Fig. 12j), 2) a magmatic null in the southern YB coupled with normal I-type calc-alkaline and adakite-like granitoid magmatism in the STB during the latest Carboniferous (~310 to ~300 Ma) (e.g., ST18, 34 and 35 in Fig. 2a) at the ongoing collision stage (Fig. 12k) and 3) high-flux magmatism with compositional diversity, as represented by normal I-type, adakite-like, S-type, A2-type and highly fractionated felsic rocks and subordinated mafic rocks, in both southern YB and STB since the earliest Permian, due to extensional regimes following slab breakoff and/or lithospheric delamination (Fig. 12l). Such a scenario is analogous to the magmatic record of India-Asia collision (Zhu et al., 2015, 2017). Besides, a latest Carboniferous to Early Permian peraluminous magmatic belt (including rocks with nos. ST20, 33 and 43 in Fig. 2a) has been recently recognized from Wensu County to Korla City in the southern STB, and the formation of this belt was likely related to partial melting of supracrustal rocks from a passive continental margin of the Tarim Craton during rapid erosional and exhumation processes (Cheng et al., 2017). Taken together, the latest Carboniferous to Early Permian magmatism in the STB likely recorded a post-collisional extensional regime following the Late Carboniferous closure of the South Tianshan Ocean.

Systemic paleomagnetic studies of Carboniferous and Permian strata indicate that there was an insignificant latitudinal difference between the Tarim, Yili, Junggar, and Siberia blocks since the late Carboniferous (Wang et al., 2007a; Zhu et al., 2018a). This, in combination with intense dextral shearing between ~309 and ~269 Ma identified in the North Tianshan Belt (Shu et al., 2002; Laurent-Charvet et al., 2003; Zhou et al., 2001; de Jong et al., 2009; Yang et al., 2009; Zhu, 2011; Xu et al., 2011; Cai et al., 2012; see compilation in Han and Zhao, 2018) implies intra-continental adjustment in the northern part of the Western Tianshan since the latest Carboniferous. The exclusive occurrence of regional-scale A-type granitic magmatism in the North Tianshan Belt since ~303 Ma (Fig. 2a) further indicates a "non-arc" tectonic setting in which decompression melt component becomes dominant (Collins et al., 2019). Taken together, we suggest that a collisional event likely occurred in the latest Carboniferous along the North Tianshan suture zone. In contrast to that of the South Tianshan Ocean, the closure of the North Tianshan Ocean in the Chinese Western Tianshan was plausibly followed by an arc-continent collision without the arrival of a micro-continent or craton with an ancient basement. The terrane collided with the northern margin of the Yili Block was likely the western extension of the Harlik-Dananhu Arc in the eastern Tianshan and thereby had an immature/nascent island arc affinity (Mao et al., 2019; Xiao et al., 2013, and references therein) (Fig. 12c and k). Highly positive εHf and εNd values and low Nb/La ratios (Fig. 3i, 4, and 7b) presented in latest Carboniferous to Early Permian A2-type granites in the North Tianshan Belt are in agreement with the dominance of juvenile arc-type source(s), supporting the "soft" continent-arc collision model.

In summary, the amalgamation of the Chinese Western Tianshan can be summarized as a continent-continent collision in the south and a continent-arc collision in the north. In the context of supercontinental cycles, the Late Paleozoic history of the SW CAOB was a part of the Pangea assembly (Cawood and Buchan, 2007; Wilhem et al., 2012; Wang et al., 2018d). In this view, the South Tianshan Belt and southern Yili Block can be classified a part of "internal orogen" of Pangea in which the lower crust (and lithospheric mantle) is eventually replaced by an older continental lithosphere from a collided continental fragment (Collins et al., 2011). By contrast, the scenario of North Tianshan Belt and northern YB was more comparable to that of the "external orogenic system" (e.g., Circum-Pacific accretionary orogens), as a trapped/remnant oceanic basin likely still exist even after the arc-continent collisional event (Fig. 12c; Han and Zhao, 2018).

7.5. Implications for the formation of the Kazakhstan Orocline

The Late Paleozoic history of the SW CAOB was closely associated with the oroclinal bending and tightening of the originally quasi-linear Kazakhstan micro-continent (Windley et al., 2007; Xiao and Santosh, 2014; Xiao et al., 2015, 2018; Li et al., 2018, 2019; Yakubchuk, 2017). The Yili Block constitute the major part of the southern limb of the Kazakhstan orocline (Han and Zhao, 2018). The bending of the Kazakhstan orocline most likely commenced in the Middle Devonian and was not completed until the Late Permian according to recent paleomagnetic data (e.g., Van der Voo et al., 2006; Wang et al., 2007a; Abrajevitch et al., 2008; Choulet et al., 2011, 2012; Levashova et al., 2012; Li et al., 2018; Zhu et al., 2018a), and invoke internal effects induced by asymmetric slab rollback of subducting Junggar oceanic plate (Li et al., 2018, 2019; Xiao et al., 2018), and/or buckling of a relatively linear belt in response to the convergence and collision of the Tarim and Siberia continents (e.g., Sengör et al., 1993; Allen and Natal'in, 1995; Windley et al., 2007; Abrajevitch et al., 2008; Xiao et al., 2010).

According to paleomagnetic data compiled by Levashova et al. (2012), Yi et al. (2015), Li et al. (2018) and Zhu et al. (2018a), ~112–126° clockwise rotation for the North branch of the orocline with respect to the South branch were obtained in the Late Devonian to Early Carboniferous (Fig. 12b), and a further ~15–28° clockwise rotation of the northern limb and ~39–40° anticlockwise rotation of the southern limb with respect to the hinge of the orocline were developed during the Late Carboniferous to Late Permian (Fig. 12c) (Wang et al., 2007a; Yi et al., 2015). Most previous models imply that the southern limb was pinned or fixed before the Late Carboniferous. In a recently proposed model by Li et al. (2018), the pinning of the southern limb was attributed to flat or advancing subduction of the North Tianshan Ocean. However, it is worth noting that few paleomagnetic data have been reported for pre-Late Carboniferous rocks in the Yili Block (e.g., Wang et al., 2007a). As mentioned above, the newly published geochronological data of detrital zircons and granitic rocks argues for continuous retreat subduction of the North Tianshan Ocean during the latest Devonian to Early Carboniferous, without recognizable magmatic hiatus in the northern margin of the YB. In this case, whether the southern limb of the orocline was being "pined" before the Late Carboniferous is still an open question. More paleomagnetic investigations need to be carried out on pre-Late Carboniferous rocks, and the combined effect of both northward trench retreat of the North Tianshan Ocean and southward trench retreat of the South Tianshan Ocean during the latest Devonian to Early Carboniferous should be taken into consideration.

The amalgamation of the Yili Block and Tarim Craton coincided with the significant anticlockwise rotation. During the initial stage of the collision, the rate of retreat of the North Tianshan oceanic plate was likely higher than the convergence rate of the Tarim Craton, thus leading to the development of back-arc extensional basin and formation of some large-sized submarine volcanic-hosted iron deposits in the present Awulale Mountains during ~320 to ~310 Ma, as described above. Thus, trench retreat that provided trench suction force, was the primary factor in the bending of the southern limb in the short period. Subsequently, the ongoing collision (~310 to ~300 Ma) was accompanied by the closure of back-arc basins, implying that the convergence in the south became faster than the retreat of the North Tianshan Ocean in the north. Coeval with anticlockwise rotation, significant strike-slip movements and dextral shearing developed in the West Tiansahn during the Early Permian to the earliest Triassic (Section 7.4; Li et al., 2018; Zhou et al., 2018). In this scenario, the continent-continent amalgamation likely played a significant role in oroclinal bending since the latest Carboniferous.

7.6. Broader implications for the formation and preservation of juvenile crust of the CAOB

In the Central Asian Orogenic Belt, remnants of juvenile materials generated in oceanic crust, intra-oceanic arcs, ocean islands and oceanic plateaus in mélanges in accretionary wedges indicate significant lateral continental growth (Windley et al., 2007; Kröner et al., 2014, 2017; Safonova, 2017; Yang et al., 2019). In some juvenile terranes without an ancient basement, intermediate to felsic magmatism originated from the partial melting of the remnant oceanic crust was another mechanism of continental growth (Xu et al., 2013c; Xu et al., 2016). However, whether extensive juvenile additions associated with accretionary orogenesis occurred and are still preserved in the micro-continents of the CAOB is still a controversial issue.

The current study highlights the importance of supra-subduction extension triggered by trench retreat (slab rollback) in the continental growth of the Yili Block and adjacent regions. On a larger scale, such a long-term "rejuvenation" process, characterized by the gradual replacement of pre-accretionary Precambrian basement by syn-accretionary juvenile crust, associated with subduction zone retreat (rollback) has been documented in some other micro-continents of the CAOB, such as those in Eastern Tianshan (Zhang et al., 2019b), Beishan (Song et al., 2015; He et al., 2018), and Mongolian Altai (Guy et al., 2015). Therefore, presently preserved crust within many micro-continents of the CAOB can be preferentially classified as mixtures between old pre-accretionary and juvenile syn-accretionary components. As the collision between continental crustal fragments would replace the lower crust and lithospheric mantle beneath the accretionary wedge and, possibly, overriding continental margin with older continental lithosphere (Collins et al., 2011), the preservation of juvenile/mixed crust requires some continental margins that did not collide with an ancient micro-continent or craton (i.e., non-collisional or soft-collisional margins) even until the termination of accretionary orogenesis (Mišković and Schaltegger, 2009). As exemplified by the case of the northern Yili Block and North Tianshan Belt, development of a series of oroclines, e.g., the Kazakhstan Orocline in the west and the Tuva-Mongol Orocline in the east (Xiao et al., 2015, 2018; Li et al., 2018, 2019), is likely the principal mechanism resulting in trapped/remnant oceanic basins, occurrence of several non-collisional (or soft-collisional) continental margins and survival (preservation) of juvenile/mixed crust in the huge fossil orogen.

8. Conclusions

(1) The synthesis of the Hf-in-zircon isotopic dataset of Paleozoic felsic rocks in the Yili Block and adjacent regions reveal remarkable spatial and temporal heterogeneity for sources of Paleozoic felsic rocks. Spatially, Hf isotopic mapping unveils an inboard-younging trend in crustal Hf model age of the Yili Block, which indicates relative ancient basement rocks interspersing in its northern and southern edges and the most juvenile crust beneath its centre. Temporally, the compiled zircon Hf isotopic dataset suggests alternating continental reworking and growth in the Yili and adjacent regions during Paleozoic times.

(2) The prolonged subduction of branches of the Paleo-Asian Ocean, i.e., the North Tianshan Ocean in the north and the South Tianshan Ocean in the south, can be temporarily divided to two stages (mainly from ~460 to ~395 Ma and from ~375 to ~310 Ma, respectively), and was featured by periodic trench advance and retreat. In the first-stage subduction, the tectonic switch from advancing to retreating subduction likely took place around ~450 Ma in the northern Yili Block and ~420 Ma in the southern Yili Block. The second-stage subduction was characterized by a period of trench advance (~ 375 to ~350 Ma in the northern Yili Block and ~370 to ~350 Ma in the southern Yili Block) at the initiation and the following Early Carboniferous trench retreat (~350 to ~310 Ma in the northern Yili Block, and ~350 to ~322 Ma in the southern Yili Block) associated with the development of back-arc basins.

(3) The final assembly of the Western Tianshan orogenic collage plausibly occurred during the Late Carboniferous. In the south, a "hard" collision followed the closure of the South Tianshan Ocean. On the contrary, the northern margin of the YB was likely collided "softly" with an immature/nascent island arc. In the context of the assembly of Pangea, the South Tianshan Belt and southern Yili Block was a part of "internal orogen" of Pangea, whereas the North Tianshan Belt and northern Yili Block was more comparable to that of the "external orogenic system", as a trapped/remnant oceanic basin likely still exist even after the arc-continent collisional event.

(4) The current study highlights the importance of supra-subduction extension triggered by trench retreat (slab rollback) in the continental growth of the Yili Block and adjacent regions. On a larger scale, the long-term "rejuvenation" process that was characterized by the gradual replacement of the old basement by juvenile crust and associated with subduction zone retreat (rollback) has been documented in several micro-continents of the CAOB. Development of some oroclines, e.g., the Kazakhstan Orocline in the west and the Tuva-Mongol Orocline in the east, plausibly played an essential role in preserving juvenile/mixed crust within the huge fossil orogen.

Declaration of competing interest

The authors declare that they have no known competing financial interests or personal relationships that could have appeared to influence the work reported in this paper.

Acknowledgments

The authors are grateful to Editor Dr. Arturo Gomez-Tuena and two anonymous referees for constructive suggestions and comments which helped to improve our paper. He Huang and Qie Qin thank Yanguang Li of the Center of Experimental Tests, Xi'an Center of Geological Survey, and Zhaochu Hu and Lei Xu of the State Key Laboratory of Geological Processes and Mineral Resources, China University of Geosciences (Wuhan) for their assistance in zircon U-Pb and Hf isotopic determinations. He Huang thank Xuezhong Yu for providing the high-resolution image file of the magnetic anomaly map, and Jiyao Hou, Jing Wang and Zhaoyuan Liang for their assistance in compiling the dataset. This study was jointly supported by National Key Technologies R&D Program (nos. 2019YFA0708601 and 2017YFC0601305), National Nature Science Foundation of China (no. 41830216) and project of the China Geological Survey (no. DD20190001), and is a contribution to IGCP Project 662.

Appendix A. Supplementary data

Supplementary data to this article can be found online at https://doi.org/10.1016/j.earscirev.2020.103255.

References

Abrajevitch, A., Van der Voo, R., Bazhenov, M.L., Levashova, N.M., McCausland, P.J.A., 2008. The role of the Kazakhstan orocline in the late Paleozoic amalgamation of Eurasia. Tectonophysics 455, 61–76.

Aitchison, J.C., Buckman, S., 2012. Accordion vs. quantum tectonics: insights into continental growth processes from the Paleozoic of eastern Gondwana. Gondwana Res. 22, 674–680.

Alekseev, D.V., Degtyarev, K.E., Kotov, A.B., Sal Nikova, E.B., Tret Yakov, A.A., Yakovleva, S.Z., Anisimova, I.V., Shatagin, K.N., 2009. Late Paleozoic subductional and collisional igneous complexes in the Naryn segment of the Middle Tien Shan (Kyrgyzstan). Dokl. Earth Sci. 427, 760–763.

Allen, M., Natal'in, B., 1995. Junggar. Turfan and Alakol basins as Late Permian to? Early Triassic extensional structures in a sinistral shear zone in the Altaid orogenic collage, Central Asia. Journal of the Geological Society 152, 327–338.

Antonijevic, S.K., Wagner, L.S., Kumar, A., Beck, S.L., Long, M.D., Zandt, G., Tavera, H., Condori, C., 2015. The role of ridges in the formation and longevity of flat slabs.

Nature 524, 212–215.
Axen, G.J., van Wijk, J.W., Currie, C.A., 2018. Basal continental mantle lithosphere displaced by flat-slab subduction. Nature Geoscience 11, 961–964.
Bao, Z.-H., Cai, K.-D., Sun, M., Xiao, W.-J., Wan, B., Wang, Y.-N., Wang, X.-S., Xia, X.-P., 2018. Continental crust melting induced by subduction initiation of the South Tianshan Ocean: insight from the Latest Devonian granitic magmatism in the southern Yili Block, NW China. J. Asian Earth Sci. 153, 100–117.
Bazhenov, M.L., Collins, A.Q., Degtyarev, K.E., Levashova, N.M., Mikolaichuk, A.V., Pavlov, V.E., Van der Voo, R., 2003. Paleozoic northward drift of the North Tien Shan (Central Asia) as revealed by Ordovician and Carboniferous paleomagnetism. Tectonophysics 366, 113–141.
Biske, Y., Seltmann, S.R., 2010. Paleozoic Tian-Shan as a transitional region between the Rheic and Urals-Turkestan oceans. Gondwana Res. 17, 602–613.
Boekhout, F., Roberts, N.M.W., Gerdes, A., Schaltegger, U., 2015. A Hf-isotope perspective on continent formation in the south Peruvian Andes. Geol. Soc. Lond., Spec. Publ. 389, 305–321.
Bowring, S.A., Karlstrom, K.E., 1990. Growth, stabilization, and reactivation of Proterozoic lithosphere in the southwestern United States. Geology 18, 1203–1206.
Burtman, V.S., 2008. Nappes of the southern Tien Shan. Russ. J. Earth Sci. 10, 1–35.
Cai, Z.H., Xu, Z.Q., He, B.Z., Wang, R.R., 2012. Age and tectonic evolution of ductile shear zones in the eastern Tianshan-Beishan orogenic belt. Acta Petrol. Sin. 28, 1875–1895 (in Chinese with English abstract).
Cao, Y.C., Wang, B., Jahn, B.-m., Cluzel, D., Shu, L.S., Zhong, L.L., 2017. Late Paleozoic arc magmatism in the southern Yili Block (NW China): insights to the geodynamic evolution of the Balkhash – Yili continental margin, Central Asian Orogenic Belt. Lithos 278-281, 111–125.
Carroll, A.R., Graham, S.A., Hendrix, M.S., Ying, D., Zhou, D., 1995. Late Paleozoic tectonic amalgamation of northwestern China: sedimentary record of the northern Tarim, northwestern Turpan, and southern Junggar basins. Geol. Soc. Am. Bull. 107 (5), 571–594.
Carroll, A.R., Graham, S.A., Chang, E.Z., McKnight, C., 2001. Sinian through Permian tectonostratigraphic evolution of the northwestern Tarim basin, China. In: Hendrix, M.S., Davis, G.A. (Eds.), Paleozoic and Mesozoic Tectonic Evolution of Central Asia: From Continental Assembly to Intracontinental Deformation. Geological Society of America Memoir, Boulder, Colorado, pp. 47–69.
Cawood, P.A., Buchan, C., 2007. Linking accretionary orogenesis with supercontinent assembly. Earth Sci. Rev. 82, 217–256.
Cawood, P.A., Kröner, A., Collins, W.J., Kusky, T.M., Mooney, W.D., Windley, B.F., 2009. Accretionary orogens through Earth history. In: Cawood, P.A., Kröner, A. (Eds.), Earth Accretionary Systems in Space and Time. Geological Society of London, Special Publication, 318 (1)pp. 1–36.
Champion, D.C., Huston, D.L., 2016. Radiogenic isotopes, ore deposits and metallogenic terranes: novel approaches based on regional isotopic maps and the mineral systems concept. Ore Geol. Rev. 76, 229–256.
Chapman, J.B., Ducea, M.N., DeCelles, P.G., Profeta, L., 2015. Tracking changes in crustal thickness during orogenic evolution with Sr/Y: an example from the North American Cordillera. Geology 43, 919–922.
Chapman, J.B., Ducea, M.N., Kapp, P., Gehrels, G.E., DeCelles, P.G., 2017. Spatial and temporal radiogenic isotopic trends of magmatism in Cordilleran orogens. Gondwana Res. 48, 189–204.
Chapman, J., Dafov, M., Gehrels, G., Ducea, M.N., Valley, J., Ishida, A., 2018. Lithospheric architecture and tectonic evolution of the southwestern US Cordillera: constraints from zircon Hf and O isotopic data. GSA Bull. 130, 2031–2046.
Charvet, J., Shu, L.S., Laurent-Charvet, S., Wang, B., Faure, M., Cluzel, D., Chen, Y., Jong, K., 2011. Palaeozoic tectonic evolution of the Tianshan belt, NW China. Sci. China Earth Sci. 54, 166–184.
Chen, B., Arakawa, Y., 2005. Elemental and Nd-Sr isotopic geochemistry of granitoids from the West Junggar foldbelt (NW China), with implications for Phanerozoic continental growth. Geochim. Cosmochim. Acta 69 (5), 1307–1320.
Chen, C.M., Lu, H.F., Jia, D., Cai, D.S., Wu, S.M., 1999a. Closing history of the southern Tianshan oceanic basin, western China: an oblique collisional orogeny. Tectonophysics 302, 23–40.
Chen, Y.B., Hu, A.Q., Zhang, G.X., Zhang, Q.F., 1999b. Zircon U-Pb age and Nd-Sr isotopic composition of granitic gneiss and its geological implications from Precambrian window of western Tianshan, NW China. Geochimica 28, 515–520 (in Chinese with English abstract).
Chen, X.Y., Wang, Y.J., Sun, L.H., Fan, W.M., 2009. Zircon SHRIMP U-Pb dating of the granitic gneisses from Bingdaban and Laerdundaban (Tianshan Orogen) and their geological significances. Geochimica 38, 424–431 (in Chinese with English abstract).
Cheng, Z.-G., Zhang, Z.-C., Santosh, M., Zhao, Z.-Y., Chen, L.-L., 2017. Late Carboniferous to early Permian partial melting of the metasedimentary rocks and crustal reworking in the Central Asian Orogenic Belt: evidence from garnet-bearing rhyolites in the Chinese South Tianshan. Lithos 282-283, 373–387.
Cheng, Z.-G., Zhang, Z.-C., Xie, Q.-H., Hou, T., Ke, S., 2018. Subducted slab-plume interaction traced by magnesium isotopes in the northern margin of the Tarim Large Igneous Province. Earth Planet. Sci. Lett. 489, 100–110.
Choulet, F., Chen, Y., Wang, B., Faure, M., Cluzel, D., Charvet, J., Lin, W., Xu, B., 2011. Late Paleozoic paleogeographic reconstruction of Western Central Asia based upon paleomagnetic data and its geodynamic implications. J. Asian Earth Sci. 42, 867–884.
Choulet, F., Faure, M., Cluzel, D., Chen, Y., Lin, W., Wang, B., 2012. From oblique accretion to transpression in the evolution of the Altaid collage: new insights from West Junggar, northwestern China. Gondwana Res. 21, 530–547.
Collins, W.J., 2002. Hot orogens, tectonic switching, and creation of continental crust. Geology 30 (6), 535–538.
Collins, W.J., Belousova, E.A., Kemp, A.I., Murphy, J.B., 2011. Two contrasting Phanerozoic orogenic systems revealed by hafnium isotope data. Nat. Geosci. 4, 333–337.
Collins, W.J., Huang, H.-Q., Bowden, P., Kemp, A.T.I., 2019. Repeated S-I-A-type granite trilogy in the Lachlan Orogen, and geochemical contrasts with A-type granites in Nigeria: implications for petrogenesis and tectonic discrimination. Geol. Soc. Lond., Spec. Publ. 491 SP491-2018-2159.
Condie, K.C., 1999. Mafic crustal xenoliths and the origin of the lower continental crust. Lithos 46, 95–101.
Condie, K.C., 2007. Accretionary orogens in space and time. In: Hatcher Jr.R.D. (Ed.), 4-D Framework of Continental Crust. Memoir-Geological Society of America Vol. 200. pp. 145–158.
de Jong, K., Wang, B., Faure, M., Shu, L.S., Cluzel, D., Charvet, J., Ruffet, G., Chen, Y., 2009. New $^{40}Ar/^{39}Ar$ age constraints on the Late Palaeozoic tectonic evolution of the western Tianshan (Xinjiang, northwestern China), with emphasis on Permian fluid ingress. Int. J. Earth Sci. 98, 1239–1258.
del Rey, A., Deckart, K., Arriagada, C., Martínez, F., 2016. Resolving the paradigm of the late Paleozoic–Triassic Chilean magmatism: isotopic approach. Gondwana Res. 37, 172–181.
Deng, J., Wang, C., Bagas, L., Santosh, M., Yao, E., 2018. Crustal architecture and metallogenesis in the south-eastern North China Craton. Earth Sci. Rev. 182, 251–272.
Feng, W.Y., Zhu, Y.F., 2018. Petrology and geochemistry of mafic and ultramafic rocks in the north Tianshan ophiolite: implications for petrogenesis and tectonic setting. Lithos 318-319, 124–142.
Gao, J., Klemd, R., 2003. Formation of HP-LT rocks and their tectonic implications in the western Tianshan Orogen, NW China: geochemical and age constraints. Lithos 66, 1–22.
Gao, J., Li, M.S., Xiao, X.C., Tang, Y., He, G.Q., 1998. Paleozoic tectonic evolution of the Tianshan orogen, northwestern China. Tectonophysics 287, 213–231.
Gao, J., Long, L., Klemd, R., Qian, Q., Liu, D., Xiong, X., Su, W., Liu, W., Wang, Y., Yang, F., 2009. Tectonic evolution of the South Tianshan orogen and adjacent regions, NW China: geochemical and age constraints of granitoid rocks. Int. J. Earth Sci. 98, 1221–1238.
Gao, J., Klemd, R., Qian, Q., Zhang, X., Li, J., Jiang, T., Yang, Y., 2011. The collision between the Yili and Tarim blocks of the Southwestern Altaids: geochemical and age constraints of a leucogranite dike crosscutting the HP–LT metamorphic belt in the Chinese Tianshan Orogen. Tectonophysics 499, 118–131.
Gao, J., Klemd, R., Zhu, M., Wang, X., Li, J., Wan, B., Xiao, W., Zeng, Q., Shen, P., Sun, J., Qin, K., Campos, E., 2018. Large-scale porphyry-type mineralization in the Central Asian metallogenic domain: a review. J. Asian Earth Sci. 165, 7–36.
Gazel, E., Hayes, J.L., Hoernle, K., Kelemen, P., Everson, E., Holbrook, W.S., Hauff, F., Van Den Bogaard, P., Vance, E.A., Chu, S., 2015. Continental crust generated in oceanic arcs. Nat. Geosci. 8, 321–327.
Ge, R.-F., Zhu, W.-B., Zheng, B.-H., Wu, H.-L., He, J.-W., Zhu, X.-Q., 2012a. Early Pan-African magmatism in the Tarim Craton: insights from zircon U–Pb–Lu–Hf isotope and geochemistry of granitoids in the Korla area, NW China. Precambrian Res. 212-213, 117–138.
Ge, R.F., Zhu, W.B., Wu, H.L., Zheng, B.L., Zhu, X.Q., He, J.W., 2012b. The Paleozoic northern margin of the Tarim Craton: passive or active? Lithos 142-143, 1–15.
Ge, R.F., Zhu, W.B., Wilde, S.A., He, J.W., Cui, X., Wang, X., Bihai, Z., 2014. Neoproterozoic to Paleozoic long-lived accretionary orogeny in the northern Tarim Craton. Tectonics 33, 302–329.
Ge, S., Zhai, M., Safonova, I., Li, D., Zhu, X., Zuo, P., Shan, H., 2015. Whole-rock geochemistry and Sr–Nd–Pb isotope systematics of the Late Carboniferous volcanic rocks of the Awulale metallogenic belt in the western Tianshan Mountains (NW China): petrogenesis and geodynamical implications. Lithos 228-229, 62–77.
Gutscher, M.A., Eissen, J., Bourdon, E., 2000. Can slab melting be caused by flat subduction? Geology 28, 535–538.
Guy, A., Schulmann, K., Janoušek, V., Štípská, P., Armstrong, R., Belousova, E., Dolgopolova, A., Seltmann, R., Lexa, O., Jiang, Y., 2015. Geophysical and geochemical nature of relaminated arc-derived lower crust underneath oceanic domain in southern Mongolia. Tectonics 34, 1030–1053.
Han, Y.G., Zhao, G.C., 2018. Final amalgamation of the Tianshan and Junggar orogenic collage in the southwestern Central Asian Orogenic Belt: constraints on the closure of the Paleo-Asian Ocean. Earth Sci. Rev. 186, 129–152.
Han, B.F., Wang, S.G., Jahn, B.M., Hong, D.W., Kagami, H., Sun, Y.L., 1997. Depleted mantle magma source for the Ulungur River A–type granites from North Xinjiang China: geochemistry and Nd–Sr isotopic evidence, and implication for Phanerozoic crustal growth. Chem. Geol. 138 (3–4), 135–159.
Han, B.-F., Guo, Z.-J., Zhang, Z.-C., Zhang, L., Chen, J.-F., Song, B., 2010. Age, geochemistry, and tectonic implications of a late Paleozoic stitching pluton in the North Tian Shan suture zone, western China. Geol. Soc. Am. Bull. 122, 627–640.
Han, B.-F., He, G.-Q., Wang, X.-C., Guo, Z.-J., 2011. Late Carboniferous collision between the Tarim and Kazakhstan–Yili terranes in the western segment of the South Tian Shan Orogen, Central Asia, and implications for the Northern Xinjiang, western China. Earth Sci. Rev. 109, 74–93.
Han, Y.G., Zhao, G.C., Sun, M., Eizenhöfer, P.R., Hou, W.Z., Zhang, X.R., Liu, D.X., Wang, B., Zhang, G.W., 2015. Paleozoic accretionary orogenesis in the Paleo-Asian Ocean: insights from detrital zircons from Silurian to Carboniferous strata at the northwestern margin of the Tarim Craton. Tectonics 34, 334–351.
Hao, L.-L., Wang, Q., Zhang, C., Ou, Q., Yang, J.-H., Dan, W., Jiang, Z.-Q., 2018. Oceanic plateau subduction during closure of the Bangong-Nujiang Tethyan Ocean: insights from central Tibetan volcanic rocks. GSA Bull. 131, 864–880.
He, J.W., Zhu, W.B., Ge, R.F., 2014. New age constraints on Neoproterozoic diamictites in Kuruktag, NW China and Precambrian crustal evolution of the Tarim Craton. Precambrian Res. 241, 44–60.
He, Z.-Y., Wang, B., Zhong, L.-L., Zhu, X.-Y., 2018. Crustal evolution of the Central Tianshan Block: insights from zircon U-Pb isotopic and structural data from meta-

sedimentary and meta-igneous rocks along the Wulasitai – Wulanmoren shear zone. Precambrian Res. 314, 111–128.
Hegner, E., Alexeiev, D.V., Willbold, M., Kröner, A., Topuz, G., Mikolaichuk, A.V., 2019. Early Silurian tholeiitic-boninitic Mailisu ophiolite, South Tianshan, Kyrgyzstan: a geochemical record of subduction initiation. Int. Geol. Rev. 1–18.
Hou, Z.Q., Duan, L.F., Lu, Y.J., Zheng, Y.C., Zhu, D.C., Yang, Z.M., Yang, Z.S., Wang, B.D., Pei, Y.R., Zhao, Z.D., McCuaig, T.C., 2015. Lithospheric architecture of the Lhasa Terrane and its control on ore deposits in the Himalayan–Tibetan Orogen. Econ. Geol. 110, 1541–1575.
Hu, A.Q., Jahn, B.M., Zhang, G.X., Chen, Y.B., Zhang, Q.F., 2000. Crustal evolution and Phanerozoic crustal growth in northern Xinjiang: Nd isotopic evidence. Part. I. Isotopic characterization of basement rocks. Tectonophysics 328, 15–51.
Hu, A.Q., Wei, G.J., Jahn, B.M., Zhang, J.B., Deng, W.F., Chen, L.L., 2010. Formation of the 0.9 Ga Neoproterozoic granitoids in the Tianshan Orogen, NW China: constraints from the SHRIMP zircon age determination and its tectonic significance. Geochimica 39 (3), 197–212 (in Chinese with English abstract).
Huang, H., Zhang, Z.C., Santosh, M., Zhang, D.Y., Zhao, Z.D., Liu, J.L., 2013. Early Paleozoic tectonic evolution of the South Tianshan collisional belt: evidence from geochemistry and zircon U-Pb geochronology of the Tie'reke Monzonite Pluton, Northwest China. The Journal of Geology 121, 401–424.
Huang, H., Zhang, Z., Santosh, M., Zhang, D., Wang, T., 2015a. Petrogenesis of the Early Permian volcanic rocks in the Chinese South Tianshan: implications for crustal growth in the Central Asian Orogenic Belt. Lithos 228-229, 23–42.
Huang, H., Wang, T., Qin, Q., Hou, J., Tong, Y., Guo, L., Zhang, L., Wang, J., Liang, Z., 2015b. Zircon Hf isotope characteristics of granitoids from the Baluntai region, Central Tianshan: implications for tectonic evolution and continental growth. Acta Geol. Sin. 89, 2286–2313 (in Chinese with English abstract).
Huang, Z.Y., Long, X.P., Wang, X.C., Zhang, Y.Y., Du, L., Yuan, C., Xiao, W.J., 2017a. Precambrian evolution of the Chinese Central Tianshan Block: constraints on its tectonic affinity to the Tarim Craton and responses to supercontinental cycles. Precambrian Res. 295, 24–37.
Huang, H., Niu, Y.-L., Mo, X.-X., 2017b. Garnet effect on Nd-Hf isotope decoupling: evidence from the Jinfosi batholith, Northern Tibetan Plateau. Lithos 274-275, 31–38.
Huang, H., Cawood, P.A., Ni, S., Hou, M., Shi, Z., Hu, X., 2018. Provenance of late Paleozoic strata in the Yili Basin: implications for tectonic evolution of the South Tianshan orogenic belt. GSA Bull. 130, 952–974.
Huang, H., Zhang, Z.-C., Santosh, M., Cheng, Z.-G., Wang, T., 2019a. Crustal evolution in the South Tianshan Terrane: constraints from detrital zircon geochronology and implications for continental growth in the Central Asian Orogenic Belt. Geol. J. 54, 1379–1400.
Huang, Z.-Y., Yuan, C., Long, X.-P., Zhang, Y.-Y., Du, L., 2019b. From breakup of nuna to assembly of rodinia: a link between the chinese central tianshan block and fennoscandia. Tectonics 38, 4378–4398.
Ionov, D.A., Blichert-Toft, J., Weis, D., 2005. Hf isotope compositions and HREE variations in off-craton garnet and spinel peridotite xenoliths from central Asia. Geochim. Cosmochim. Acta 69 (9), 2399–2418.
Jahn, B.M., 2004. The Central Asian Orogenic Belt and growth of the continental crust in the Phanerozoic. Geol. Soc. Lond., Spec. Publ. 226 (1), 73–100.
Jahn, B.M., Wu, F.Y., Chen, B., 2000a. Granitoids of the Central Asian Orogenic Belt and continental growth in the Phanerozoic. Trans. R. Soc. Edinb. Earth Sci. 91 (1–2), 181–193.
Jahn, B.M., Wu, F.Y., Chen, B., 2000b. Massive granitoid generation in Central Asia: Nd isotope evidence and implication for continental growth in the Phanerozoic. Episodes 23 (2), 82–92.
Jenkins, R.B., Landenberger, B., Collins, W.J., 2002. Late Palaeozoic retreating and advancing subduction boundary in the New England Fold Belt, New South Wales. Aust. J. Earth Sci. 49 (3), 467–489.
Ji, Z., Meng, Q.-A., Wan, C.-B., Zhu, D.-F., Ge, W.-C., Zhang, Y.-L., Yang, H., Dong, Y., 2019. Geodynamic evolution of Flat-Slab subduction of Paleo-Pacific Plate: constraints from Jurassic Adakitic Lavas in the Hailar Basin, NE China. Tectonics 38, 4301–4319.
Jiang, T., Gao, J., Klemd, R., Qian, Q., Zhang, X., Xiong, X., Wang, X., Tan, Z., Chen, B., 2014. Paleozoic ophiolitic mélanges from the South Tianshan Orogen, NW China: geological, geochemical and geochronological implications for the geodynamic setting. Tectonophysics 612-613, 106–127.
Jung, S., Masberg, P., Mihm, D., Hoernes, S., 2009. Partial melting of diverse crustal sources—constraints from Sr–Nd–O isotope compositions of quartz diorite–-granodiorite–leucogranite associations (Kaoko Belt, Namibia). Lithos 111 (3-4), 236–251.
Kay, S.M., Godoy, E., Kurtz, A., 2005. Epidsodic arc migration, crustal thickening, subduction erosion, and magmatism in the south-central Andes. Geol. Soc. Am. Bull. 117, 67–88.
Kemp, A.I.S., Hawkesworth, C.J., Collins, W.J., Gray, C.M., Blevin, P.L., 2009. Isotopic evidence for rapid continental growth in an extensional accretionary orogen: the Tasmanides, eastern Australia. Earth Planet. Sci. Lett. 284 (3-4), 455–466.
Konopelko, D., Biske, G., Seltmann, R., Eklund, O., Belyatsky, B., 2007. Hercynian post-collisional A-type granites of the Kokshaal Range, Southern Tien Shan, Kyrgyzstan. Lithos 97, 140–160.
Konopelko, D., Biske, G., Seltmann, R., Kiseleva, M., Matukov, D., Sergeev, S., 2008. Deciphering Caledonian events: timing and geochemistry of the Caledonian magmatic arc in the Kyrgyz Tien Shan. J. Asian Earth Sci. 32, 131–141.
Konopelko, D., Seltmann, R., Biske, G., Lepekhina, E., Sergeev, S., 2009. Possible source dichotomy of contemporaneous post-collisional barren I-type versus tin-bearing A-type granites, lying on opposite sides of the South Tien Shan suture. Ore Geol. Rev. 35, 206–216.
Kovalenko, V.I., Yarmolyuk, V.V., Kovach, V.P., Kotov, A.B., Kozakov, I.K., Salnikova, E.B., Larin, A.M., 2004. Isotope provinces, mechanisms of generation and sources of the continental crust in the Central Asian mobile belt: geological and isotopic evidence. J. Asian Earth Sci. 23, 605–627.
Kröner, A., Kovach, V., Belousova, E., Hegner, E., Armstrong, R., Dolgopolova, A., Seltmann, R., Alexeiev, D.V., Hoffmann, J.E., Wong, J., Sun, M., Cai, K., Wang, T., Tong, Y., Wilde, S.A., Degtyarev, K.E., Rytsk, E., 2014. Reassessment of continental growth during the accretionary history of the Central Asian Orogenic Belt. Gondwana Res. 25, 103–125.
Kröner, A., Kovach, V., Alexeiev, D., Wang, K.-L., Wong, J., Degtyarev, K., Kozakov, I., 2017. No excessive crustal growth in the Central Asian Orogenic Belt: further evidence from field relationships and isotopic data. Gondwana Res. 50, 135–166.
Laurent-Charvet, S., Charvet, J., Shu, L.S., Ma, R.S., Lu, H.F., 2002. Palaeozoic late collisional strike-slip deformations in Tianshan and Altay, eastern Xinjiang, NW China. Terra Nova 14 (4), 249–256.
Laurent-Charvet, S., Charvet, J., Monié, P., Shu, L.S., 2003. Late Paleozoic strike-slip shear zones in eastern Central Asia (NW China): new structural and geochronological data. Tectonics 22 (2), 1009.
Lei, R.X., Wu, C.Z., Gu, L.X., Zhang, Z.Z., Chi, G.X., Jiang, Y.H., 2011. Zircon U-Pb chronology and Hf isotope of the Xingxingxia granodiorite from the Central Tianshan zone (NW China): implications for the tectonic evolution of the southern Altaids. Gondwana Res. 20, 582–593.
Levashova, N.M., Degtyarev, K., Bazhenov, M., 2012. Oroclinal bending of the Middle and Late Paleozoic volcanic belts in Kazakhstan: paleomagnetic evidence and geological implications. Geotectonics 46, 285–302.
Li, J.Y., He, G.Q., Xu, X., Li, H.Q., Sun, G.H., Yang, T.N., Gao, L.M., Zhu, Z.X., 2006. Crustal tectonic framework of northern Xinjiang and adjacent regions and its formation. Acta Geol. Sin. 80, 148–168 (in Chinese with English abstract).
Li, C., Xiao, W.J., Han, C.M., Zhou, K.F., Zhang, J.E., Zhang, Z.X., 2015a. Late Devonian-early Permian accretionary orogenesis along the North Tianshan in the southern Central Asian Orogenic Belt. Int. Geol. Rev. 57, 1023–1050.
Li, Y.J., Wen, L., Yang, H.J., Zhang, G.Y., Shi, J., Peng, G.X., Hu, J.F., Luo, J.C., Huang, Z.B., Chen, Y.G., 2015b. New discovery and geological significance of Late Silurian-Carboniferous extensional structures in Tarim Basin. J. Asian Earth Sci. 98, 304–319.
Li, Y.J., Wu, L., Li, S.L., Li, G.Y., Shen, R., Li, Z., Wang, Z.Y., Wang, Z.Y., 2017. Tectonic evolution of Yining Block: insights from Carboniferous volcanic rocks. Acta Petrol. Sin. 33, 1–15 (in Chinese with English abstract).
Li, P., Sun, M., Rosenbaum, G., Yuan, C., Safonova, I., Cai, K., Jiang, Y., Zhang, Y., 2018. Geometry, kinematics and tectonic models of the Kazakhstan Orocline, Central Asian Orogenic Belt. J. Asian Earth Sci. 153, 42–56.
Li, P.-F., Sun, M., Shu, C.-T., Yuan, C., Jiang, Y.-D., Zhang, L., Cai, K.-D., 2019. Evolution of the Central Asian Orogenic Belt along the Siberian margin from Neoproterozoic-Early Paleozoic accretion to Devonian trench retreat and a comparison with Phanerozoic eastern Australia. Earth Sci. Rev. 198, 102951.
Lister, G., Forster, M., 2009. Tectonic mode switches and the nature of orogenesis. Lithos 113 (1–2), 274–291.
Liu, D.D., Jolivet, M., Yang, W., Zhang, Z.Y., Cheng, F., Zhu, B., Guo, Z.J., 2013. Latest Paleozoic–Early Mesozoic basin–range interactions in South Tian Shan (northwest China) and their tectonic significance: constraints from detrital zircon U–Pb ages. Tectonophysics 599, 197–213.
Long, X.-P., Yuan, C., Sun, M., Zhao, G.-C., Xiao, W.-J., Wang, Y.-J., Yang, Y.-H., Hu, A.-Q., 2010. Archean crustal evolution of the northern Tarim craton, NW China: zircon U–Pb and Hf isotopic constraints. Precambrian Res. 180, 272–284.
Long, L.-L., Gao, J., Klemd, R., Beier, C., Qian, Q., Zhang, X., Wang, J.-B., Jiang, T., 2011. Geochemical and geochronological studies of granitoid rocks from the Western Tianshan Orogen: implications for continental growth in the southwestern Central Asian Orogenic Belt. Lithos 126, 321–340.
Long, X.P., Sun, M., Yuan, C., Kröner, A., Hu, A.Q., 2012. Zircon REE patterns and geochemical characteristics of Paleoproterozoic anatectic granite in the northern Tarim Craton, NW China: implications for the reconstruction of the Columbia supercontinent. Precambrian Res. 222-223, 474–487.
Lu, S.N., Li, H.K., Zhang, C.L., Niu, G.H., 2008. Geological and geochronological evidence for the Precambrian evolution of the Tarim Craton and surrounding continental fragments. Precambrian Res. 160 (1–2), 94–107.
Ma, X.X., Shu, L.S., Meert, J.G., Li, J.Y., 2014. The Paleozoic evolution of Central Tianshan: geochemical and geochronological evidence. Gondwana Res. 25, 797–819.
Ma, X.X., Shu, L.S., Jahn, B.-M., Zhu, W.B., Faure, M., 2012. Precambrian tectonic evolution of Central Tianshan, NW China: Constraints from U–Pb dating and in situ Hf isotopic analysis of detrital zircons. Precambrian Research 222–223, 450–473.
Ma, X.X., Shu, L.S., Meert, J.G., 2015. Early Permian slab breakoff in the Chinese Tianshan belt inferred from the post-collisional granitoids. Gondwana Res. 27, 228–243.
Mamani, M., Worner, G., Sempere, T., 2010. Geochemical variations in igneous rocks of the central Andean orocline (13°S to 18°S): tracing crustal thickening and magma generation through time and space. Geol. Soc. Am. Bull. 122 (1-2), 162–182.
Mao, Q., Wang, J., Xiao, W., Windley, B.F., Schulmann, K., Yu, M., Fang, T., Li, Y., 2019. Mineralization of an intra-oceanic arc in an accretionary orogen: insights from the Early Silurian Honghai volcanogenic massive sulfide Cu-Zn deposit and associated adakites of the Eastern Tianshan (NW China). GSA Bull. 131, 803–830.
Maruyama, S., Liou, J.G., Terbayashi, M., 1996. Blueschist and eclogites of the world, and their exhumation. Int. Geol. Rev. 38, 485–594.
Mišković, A., Schaltegger, U., 2009. Crustal growth along a non-collisional cratonic margin: a Lu–Hf isotopic survey of the Eastern Cordilleran granitoids of Peru. Earth Planet. Sci. Lett. 279, 303–315.
Mole, D.R., Fiorentini, M.L., Thebaud, N., Cassidy, K.F., McCuaig, T.C., Kirkland, C.L., Romano, S.S., Doublier, M.P., Belousova, E.A., Barnes, S.J., Miller, J., 2014. Archean

komatiite volcanism controlled by the evolution of early continents. Proc. Natl. Acad. Sci. 111 (28), 10083–10088.
Nelson, D.A., Cottle, J.M., 2017. Long-term geochemical and geodynamic segmentation of the Paleo-Pacific Margin of Gondwana: insight from the Antarctic and Adjacent Sectors. Tectonics 36 (12), 3229–3247.
Niu, Y.L., 2018. Geological understanding of plate tectonics: basic concepts, illustrations, examples and new perspectives. Global Tectonics Metallog. 10, 23–46.
Patchett, P.J., White, W.M., Feldmann, H., Kielinczuk, S., Hofmann, A.W., 1984. Hafnium/rare earth element fractionation in the sedimentary system and crustal recycling into the Earth's mantle. Earth Planet. Sci. Lett. 69 (2), 365–378.
Pearce, J.A., Peate, D.W., 1995. Tectonic implications of the composition of volcanic arc magmas. Annu. Rev. Earth Planet. Sci. 23, 251–285.
Phillips, G., Landenberger, B., Belousova, E.A., 2011. Building the New England Batholith, eastern Australia—Linking granite petrogenesis with geodynamic setting using Hf isotopes in zircon. Lithos 122, 1–12.
Profeta, L., Ducea, M.N., Chapman, J.B., Paterson, S.R., Gonzales, S.M., Kirsch, M., Petrescu, L., DeCelles, P.G., 2015. Quantifying crustal thickness over time in magmatic arcs. Sci. Rep. 5, 17786.
Qian, Q., Gao, J., Klemd, R., He, G.-Q., Song, B., Liu, D.-Y., Xu, R.-H., 2007. Early Paleozoic tectonic evolution of the Chinese South Tianshan Orogen: constraints from SHRIMP zircon U–Pb geochronology and geochemistry of basaltic and dioritic rocks from Xiate, NW China. Int. J. Earth Sci. 98, 551–569.
Ren, R., Han, B.-F., Ji, J.-Q., Zhang, L., Xu, Z., Su, L., 2011. U–Pb age of detrital zircons from the Tekes River, Xinjiang, China, and implications for tectonomagmatic evolution of the South Tian Shan Orogen. Gondwana Res. 19, 460–470.
Rojas-Agramonte, Y., Kröner, A., Demoux, A., Xia, X., Wang, W., Donskaya, T., Liu, D., Sun, M., 2011. Detrital and xenocrystic zircon ages from Neoproterozoic to Palaeozoic arc terranes of Mongolia: significance for the origin of crustal fragments in the Central Asian Orogenic Belt. Gondwana Res. 19, 751–763.
Royden, L.H., 1993. The tectonic expression slab pull at continental convergent boundaries. Tectonics 12 (2), 303–325.
Rudnick, R.L., 1995. Making continental crust. Nature 378, 573–578.
Safonova, I., 2017. Juvenile versus recycled crust in the Central Asian Orogenic Belt: implications from ocean plate stratigraphy, blueschist belts and intra-oceanic arcs. Gondwana Res. 47, 6–27.
Safonova, I.Y., Santosh, M., 2014. Accretionary complexes in the Asia-Pacific region: tracing archives of ocean plate stratigraphy and tracking mantle plumes. Gondwana Res. 25 (1), 126–158.
Santosh, M., Maruyama, S., Komiya, T., Yamamoto, S., 2010. Orogens in the evolving earth: from surface continents to 'lost continents' at the core–mantle boundary. In: Kusky, T., Zhai, M.-G., Xiao, W. (Eds.), The Evolving Continents: Understanding Processes of Continental Growth. Geological Society, London, Special Publications Vol. 338. pp. 77–116.
Schmidberger, S.S., Simonetti, A., Francis, D., Gariépy, C., 2002. Probing archean lithosphere using the Lu-Hf isotope systematics of peridotite xenoliths from Somerset Island Kimberlites, Canada. Earth Planet. Sci. Lett. 197 (3/4), 245–259.
Sengör, A.M.C., Natal'in, B.A., Burtman, V.S., 1993. Evolution of the Altaid tectonic collage and Paleozoic crustal growth in Eurasia. Nature 364, 299–307.
Shi, Z.S., Yang, W., Guo, C.M., Zhu, X.M., Zhang, L., Chen, G., 2007. Depositional sequence and filling response characteristics of Silurian in Tarim Basin. Acta Sedimentol. Sin. 25, 401–408 (in Chinese with English abstract).
Shu, L.S., Charvet, J., Lu, H.F., Laurent-Charvet, S., 2002. Paleozoic accretion-collision events and kinematics of ductile deformation in the eastern part of the Southern-Central Tianshan Belt, China. Acta Geol. Sin. 76, 308–323.
Shu, L.S., Deng, X.L., Zhu, W.B., Ma, D.S., Xiao, W.J., 2011. Precambrian tectonic evolution of the Tarim Block, NW China: new geochronological insights from the Quruqtagh domain. J. Asian Earth Sci. 42, 774–790.
Song, D.-F., Xiao, W.-J., Windley, B.F., Han, C.-M., Tian, Z.-H., 2015. A Paleozoic Japan-type subduction-accretion system in the Beishan orogenic collage, southern Central Asian Orogenic Belt. Lithos 224-225, 195–213.
Song, P., Wang, T., Tong, Y., Zhang, J.J., Huang, H., Qin, Q., 2019. Contrasting deep crustal compositions between the Altai and East Junggar orogens, SW Central Asian Orogenic Belt: evidence from zircon Hf isotopic mapping. Lithos 328-329, 297–311.
Su, W.-B., Cai, K.-D., Sun, M., Wan, B., Wang, X.-S., Bao, Z.-H., Xiao, W.-J., 2018. Carboniferous volcanic rocks associated with back-arc extension in the western Chinese Tianshan, NW China: insight from temporal-spatial character, petrogenesis and tectonic significance. Lithos 310-311, 241–254.
Sun, S.S., McDonough, W.F., 1989. Chemical and isotopic systematics of oceanic basalts: implications for mantle composition and processes. In: Saunders, A.D., Norry, M.J. (Eds.), Magmatism in the Ocean Basins. Geol. Soc. (Lond.) Spec. Publ.pp. 313–345.
Tan, Z., Agard, P., Monié, P., Gao, J., John, T., Bayet, L., Jiang, T., Wang, X.-S., Hong, T., Wan, B., Caron, B., 2019. Architecture and P-T-deformation-time evolution of the Chinese SW-Tianshan HP/UHP complex: implications for subduction dynamics. Earth Sci. Rev. 197, 102894.
Tang, G.-J., Chung, S.-L., Hawkesworth, C.J., Cawood, P.A., Wang, Q., Wyman, D.A., Xu, Y.-G., Zhao, Z.-H., 2017a. Short episodes of crust generation during protracted accretionary processes: evidence from Central Asian Orogenic Belt, NW China. Earth Planet. Sci. Lett. 464, 142–154.
Tang, G.J., Wang, Q., Wyman, D.A., Chung, S.L., Chen, H.Y., Zhao, Z.H., 2017b. Genesis of pristine adakitic magmas by lower crustal melting: a perspective from amphibole composition. J. Geophys. Res. Solid Earth 122, 1934–1948.
Van der Voo, R., Levashova, N.M., Skrinnik, L.I., Kara, T.V., Bazhenov, M.L., 2006. Late orogenic, large-scale rotations in the Tien Shan and adjacent mobile belts in Kyrgyzstan and Kazakhstan. Tectonophysics 426, 335–360.
Vervoort, J.D., Patchett, P.J., Blichert-Toft, J., Albarède, F., 1999. Relationships between Lu–Hf and Sm–Nd isotopic systems in the global sedimentary system. Earth Planet. Sci. Lett. 168, 79–99.
Wang, B., Faure, M., Cluzel, D., Shu, L.S., Charvet, J., Meffre, S., Ma, Q., 2006. Late Paleozoic tectonic evolution of the northern West Chinese Tianshan Belt. Geodin. Acta 19, 237–247.
Wang, B., Chen, Y., Zhan, S., Shu, L., Faure, M., Cluzel, D., Charvet, J., Laurent-Charvet, S., 2007a. Primary Carboniferous and Permian paleomagnetic results from the Yili Block (NW China) and their implications on the geodynamic evolution of Chinese Tianshan Belt. Earth Planet. Sci. Lett. 263, 288–308.
Wang, Q., Wyman, D., Zhao, Z., Xu, J., Bai, Z., Xiong, X., Dai, T., Li, C., Chu, Z., 2007b. Petrogenesis of Carboniferous adakites and Nb-enriched arc basalts in the Alataw area, northern Tianshan Range (western China): implications for Phanerozoic crustal growth in the Central Asia orogenic belt. Chem. Geol. 236, 42–64.
Wang, B., Faure, M., Shu, L.-S., Cluzel, D., Charvet, J., De Jong, K., Chen, Y., 2008. Paleozoic tectonic evolution of the Yili Block, western Chinese Tianshan. Bull. Soc.Géol. France 179, 483–490.
Wang, T., Jahn, B.M., Kovach, V.P., Tong, Y., Hong, D.W., Han, B.F., 2009a. Nd–Sr isotopic mapping of the Chinese Altai and implications for continental growth in the Central Asian Orogenic Belt. Lithos 110 (1), 359–372.
Wang, B., Cluzel, D., Shu, L.S., Faure, M., Charvet, J., Chen, Y., Meffre, S., Jong, K., 2009b. Evolution of calc-alkaline to alkaline magmatism through Carboniferous convergence to Permian transcurrent tectonics, western Chinese Tianshan. Int. J. Earth Sci. 98, 1275–1298.
Wang, B., Shu, L.S., Faure, M., Jahn, B.M., Cluzel, D., Charvet, J., Chung, S.L., Meffre, S., 2011. Paleozoic tectonics of the southern Chinese Tianshan: insights from structural, chronological and geochemical studies of the Heiyingshan ophiolitic melange (NW China). Tectonophysics 497, 85–104.
Wang, B., Shu, L.-S., Liu, H.-S., Gong, H.-J., Ma, Y.-Z., Mu, L.-X., Zhong, L.-L., 2014a. First evidence for ca. 780Ma intra-plate magmatism and its implications for Neoproterozoic rifting of the North Yili Block and tectonic origin of the continental blocks in SW of Central Asia. Precambrian Res. 254, 258–272.
Wang, B., Liu, H.-S., Shu, L.-S., Jahn, B.-M., Chung, S.-L., Zhai, Y.-Z., Liu, D.-Y., 2014b. Early Neoproterozoic crustal evolution in northern Yili Block: insights from migmatite, orthogneiss and leucogranite of the Wenquan metamorphic complex in the NW Chinese Tianshan. Precambrian Res. 242, 58–81.
Wang, C.M., Bagas, L., Lu, Y.J., Santosh, M., Du, B., McCuaig, T.C., 2016. Terrane boundary and spatio-temporal distribution of ore deposits in the Sanjiang Tethyan Orogen: insights from zircon Hf-isotopic mapping. Earth Sci. Rev. 156, 39–65.
Wang, X.S., Gao, J., Klemd, R., Jiang, T., Li, J.L., Zhang, X., Xue, S.C., 2017. The Central Tianshan Block: a microcontinent with a Neoarchean-Paleoproterozoic basement in the southwestern Central Asian Orogenic Belt. Precambrian Res. 295, 130–150.
Wang, M., Zhang, J., Zhang, B., Liu, K., Chen, Y., Zheng, Y., 2018a. Geochronology and geochemistry of the Borohoro pluton in the northern Yili Block, NW China: implication for the tectonic evolution of the northern West Tianshan orogen. J. Asian Earth Sci. 153, 154–169.
Wang, M., Zhang, J., Pei, X., Liu, K., Zhang, B., Chen, Y., 2018b. Significant Carboniferous magmatism and continental growth in the northern West Tianshan orogen, NW China: revealed by detrital zircon U-Pb and Lu-Hf analyses for turbidites from the North Tianshan Accretionary Complex. J. Geodyn. 118, 11–31.
Wang, X.-S., Zhang, X., Gao, J., Li, J.-L., Jiang, T., Xue, S.-C., 2018c. A slab break-off model for the submarine volcanic-hosted iron mineralization in the Chinese Western Tianshan: insights from Paleozoic subduction-related to post-collisional magmatism. Ore Geol. Rev. 92, 144–160.
Wang, X.-S., Klemd, R., Gao, J., Jiang, T., Li, J.-L., Xue, S.-C., 2018d. Final assembly of the southwestern Central Asian Orogenic Belt as constrained by the evolution of the South Tianshan Orogen: links with Gondwana and Pangea. J. Geophys. Res. Solid Earth 123, 7361–7388.
Wang, X.-S., Cai, K.-D., Sun, M., Xiao, W.-J., Xia, X.-P., Wan, B., Bao, Z.-H., Wang, Y.-N., 2018e. Two contrasting late Paleozoic magmatic episodes in the northwestern Chinese Tianshan Belt, NW China: implication for tectonic transition from plate convergence to intra-plate adjustment during accretionary orogenesis. J. Asian Earth Sci. 153, 118–138.
Wang, Z.-P., Li, Y.-J., Tong, L.-L., Yang, G.-X., Ren, P.-F., Wang, R., Li, H., Li, S., 2018f. Identifying Early Carboniferous bimodal volcanic rocks and geochemical characteristics in the Atengtao Mountain, Yili Block (Chinese western Tianshan). Geol. J. 53, 148–162.
Wang, Z.-P., Li, Y.-J., Yang, G.-X., Tong, L.-L., Li, H., Luo, Y.-Q., Liu, Y., 2020. Petrogenesis and geochemical characteristics of Early Carboniferous sanukitic high-Mg andesite from Atengtao Mountain, Yili Block: implications for the tectonic setting during Late Palaeozoic in Chinese West Tianshan. Geol. J. 55, 517–532.
Watson, E.B., Harrison, T.M., 1983. Zircon saturation revisited: temperature and composition effects in a variety of crustal magma types. Earth Planet. Sci. Lett. 64, 295–304.
Wilde, S.A., 2015. Final amalgamation of the Central Asian Orogenic Belt in NE China: Paleo-Asian Ocean closure versus Paleo-Pacific plate subduction – a review of the evidence. Tectonophysics 662, 345–362.
Wilhem, C., Windley, B.F., Stampfli, G.M., 2012. The Altaids of Central Asia: a tectonic and evolutionary innovative review. Earth Sci. Rev. 113, 303–341.
Windley, B.F., Alexeiev, D., Xiao, W.J., Kröner, A., Badarch, G., 2007. Tectonic models for accretion of the Central Asian Orogenic Belt. J. Geol. Soc. 164, 31–47.
Wooden, J.L., Barth, A.P., Mueller, P.A., 2013. Crustal growth and tectonic evolution of the Mojave crustal province: insights from hafnium isotope systematics in zircons. Lithosphere 5, 17–28.
XBGMR (Xinjiang Bureau of Geology and Mineral Resources), 1993. Regional Geology of Xinjiang Uygur Autonomy Region. Geological Publishing House, Beijing (in Chinese).
Xia, B., Zhang, L.F., Xia, Y., Bader, T., 2014. The tectonic evolution of the Tianshan Orogenic Belt: evidence from U–Pb dating of detrital zircons from the Chinese

southwestern Tianshan accretionary mélange. Gondwana Res. 25, 1627–1643.
Xiao, W., Santosh, M., 2014. The western Central Asian Orogenic Belt: a window to accretionary orogenesis and continental growth. Gondwana Res. 25, 1429–1444.
Xiao, W.-J., Huang, B.-C., Han, C.-M., Sun, S., Li, J.-L., 2010. A review of the western part of the Altaids: a key to understanding the architecture of accretionary orogens. Gondwana Res. 18, 253–273.
Xiao, W.J., Windley, B.F., Allen, M.B., Han, C.M., 2013. Paleozoic multiple accretionary and collisional tectonics of the Chinese Tianshan orogenic collage. Gondwana Res. 23, 1316–1341.
Xiao, W.J., Han, C.M., Liu, W., Wan, B., Zhang, J.E., Ao, S.J., Zhang, Z.Y., Song, D.F., Tian, Z.H., Luo, J., 2014. How many sutures in the southern Central Asian Orogenic Belt: insights from East Xinjiang–West Gansu (NW China)? Geosci. Front. 5, 525–536.
Xiao, W.-J., Windley, B.F., Sun, S., Li, J.-L., Huang, B.-C., Han, C.-M., Yuan, C., Sun, M., Chen, H.-L., 2015. A tale of amalgamation of three Permo-Triassic collage systems in Central Asia: oroclines, sutures, and Terminal Accretion. Annu. Rev. Earth Planet. Sci. 43, 477–507.
Xiao, W.-J., Windley, B.F., Han, C.-M., Liu, W., Wan, B., Zhang, J.-E., Ao, S.-J., Zhang, Z.-Y., Song, D.-F., 2018. Late Paleozoic to early Triassic multiple roll-back and oroclinal bending of the Mongolia collage in Central Asia. Earth Sci. Rev. 186, 94–128.
Xiao, W.-J., Song, D.-F., Windley, B.F., Li, J.-L., Han, C.-M., Wan, B., Zhang, J.-E., Ao, S.-J., Zhang, Z.-Y., 2020. Accretionary processes and metallogenesis of the Central Asian Orogenic Belt: advances and perspectives. Sci. China Earth Sci. 1–33.
Xu, X.Y., Li, X.M., Ma, Z.P., Xia, L.Q., Xia, Z.C., Peng, S.X., 2006. LA-ICPMS zircon U-Pb dating of gabbro from the Bayingou ophiolite in the Northern Tianshan mountains. Acta Geol. Sin. 8, 1168–1176 (in Chinese with English abstract).
Xu, Z.Q., Li, S.T., Zhang, J.X., Sui, Y.J., He, B.Z., Li, H.B., Lin, C.S., Cai, Z.H., 2011. Paleo-Asian and Tethyan tectonic systems with docking the Tarim block. Acta Petrol. Sin. 27, 1–22 (in Chinese with English abstract).
Xu, Z.Q., He, B.Z., Zhang, C.L., Zhang, J.X., Wang, Z.M., Cai, Z.H., 2013a. Tectonic framework and crustal evolution of the Precambrian basement of the Tarim Block in NW China: new geochronological evidence from deep drilling samples. Precambrian Res. 235, 150–162.
Xu, X.-Y., Wang, H.-L., Li, P., Chen, J.-L., Ma, Z.-P., Zhu, T., Wang, N., Dong, Y.-P., 2013b. Geochemistry and geochronology of Paleozoic intrusions in the Nalati (Narati) area in western Tianshan, Xinjiang, China: implications for Paleozoic tectonic evolution. J. Asian Earth Sci. 72, 33–62.
Xu, Q.-Q., Ji, J.-Q., Zhao, L., Gong, J.-F., Zhou, J., He, G.-Q., Zhong, D.-L., Wang, J.-D., Griffiths, L., 2013c. Tectonic evolution and continental crust growth of Northern Xinjiang in northwestern China: remnant ocean model. Earth Sci. Rev. 126, 178–205.
Xu, Y.-X., Yang, B., Zhang, S., Liu, Y., Zhu, L.-P., Huang, R., Chen, C., Li, Y.-T., Luo, Y.-H., 2016. Magnetotelluric imaging of a fossil paleozoic intraoceanic subduction zone in western Junggar, NW China. J. Geophys. Res. Solid Earth 121, 4103–4117.
Yakubchuk, A., 2017. Evolution of the Central Asian orogenic supercollage since Late Neoproterozoic revised again. Gondwana Res. 47, 372–398.
Yan, S., Shan, Q., Niu, H.-C., Yang, W.-B., Li, N.-B., Zeng, L.-J., Jiang, Y.-H., 2015. Petrology and geochemistry of late Carboniferous hornblende gabbro from the Awulale Mountains, western Tianshan (NW China): implication for an arc–nascent back-arc environment. J. Asian Earth Sci. 113, 218–237.
Yang, S.H., Zhou, M.F., 2009. Geochemistry of the 430-Ma Jingbulake mafic–ultramafic intrusion in Western Xinjiang, NW China: implications for subduction related magmatism in the South Tianshan orogenic belt. Lithos 113, 259–273.
Yang, T.N., Li, J.Y., Sun, G.H., Wang, Y.B., 2006. Earlier Devonian active continental arc in Central Tianshan: evidence of geochemical analyses and Zircon SHRIMP dating on mylonitized granitic rock. Acta Geol. Sin. 22, 41–48.
Yang, T.N., Li, J.Y., Wang, Y., Dang, Y.X., 2009. Late Early Permian (266 Ma) N-S compressional deformation of the Turfan basin, NW China: the cause of the change in basin pattern. Int. J. Earth Sci. 98, 1311–1324.
Yang, G., Li, Y., Xiao, W., Tong, L., 2015. OIB-type rocks within West Junggar ophiolitic mélanges: evidence for the accretion of seamounts. Earth Sci. Rev. 150, 477–496.
Yang, G., Li, Y., Kerr, A.C., Tong, L., 2018a. Accreted seamounts in North Tianshan, NW China: implications for the evolution of the Central Asian Orogenic Belt. J. Asian Earth Sci. 153, 223–237.
Yang, G., Li, Y., Li, S., Tong, L., Wang, Z., Wu, L., Somerville, I., 2018b. Accreted seamounts in the South Tianshan Orogenic Belt, NW China. Geol. J. 53, 16–29.
Yang, G.-X., Li, Y.-J., Tong, L.-L., Wang, Z.-P., Duan, F.-H., Xu, Q., Li, H., 2019. An overview of oceanic island basalts in accretionary complexes and seamounts accretion in the western Central Asian Orogenic Belt. J. Asian Earth Sci. 179, 385–398.
Yi, Z.-Y., Huang, B.-C., Xiao, W.-J., Yang, L.-K., Qiao, Q.-Q., 2015. Paleomagnetic study of Late Paleozoic rocks in the Tacheng Basin of West Junggar (NW China): implications for the tectonic evolution of the western Altaids. Gondwana Res. 27, 862–877.
Yin, J.Y., Chen, W., Xiao, W.J., Yuan, C., Windley, B.F., Yu, S., Cai, K.D., 2017. Late Silurian–early Devonian adakitic granodiorite, A-type and I-type granites in NW Junggar, NW China: partial melting of mafic lower crust and implications for slab roll-back. Gondwana Res. 43, 55–73.
Yu, X.Z., 2016. The Characteristics of Regional Aeromagnetic & Satellite Gravity Data and Regional Metallogenic Environments, Western Tianshan, China. Ph. D. Dissertation. China University of Geological Sciences, Beijing, pp. 1–208 (in Chinese with English abstract).
Zhang, C.-L., Zou, H.-B., 2013a. Permian A-type granites in Tarim and western part of Central Asian Orogenic Belt (CAOB): genetically related to a common Permian mantle plume? Lithos 172-173, 47–60.
Zhang, C.-L., Zou, H.-B., 2013b. Comparison between the Permian mafic dykes in Tarim and the western part of Central Asian Orogenic Belt (CAOB), NW China: implications for two mantle domains of the Permian Tarim Large Igneous Province. Lithos 174, 15–27.
Zhang, C.-L., Zou, H.-B., Li, H.-K., Wang, H.-Y., 2013a. Tectonic framework and evolution of the Tarim Block in NW China. Gondwana Res. 23, 1306–1315.
Zhang, L.F., Du, J.X., Lü, Z., Yang, X., Gou, L.L., Xia, B., Chen, Z.Y., Wei, C.J., Song, S.G., 2013b. A huge oceanic-type UHP metamorphic belt in southwestern Tianshan, China: peak metamorphic age and P–T path. Chin. Sci. Bull. 58, 4378–4383.
Zhang, X.-R., Zhao, G.-C., Eizenhöfer, P.R., Sun, M., Han, Y.-G., Hou, W.-Z., Liu, D.-X., Wang, B., Liu, Q., Xu, B., 2016a. Late Ordovician adakitic rocks in the Central Tianshan block, NW China: partial melting of lower continental arc crust during back-arc basin opening. Geol. Soc. Am. Bull. 128, 1367–1382.
Zhang, X.-R., Zhao, G.-C., Sun, M., Eizenhöfer, P.R., Han, Y.-G., Hou, W.-Z., Liu, D.-X., Wang, B., Liu, Q., Xu, B., 2016b. Tectonic evolution from subduction to arc-continent collision of the Junggar ocean: constraints from U-Pb dating and Hf isotopes of detrital zircons from the North Tianshan belt, NW China. Geol. Soc. Am. Bull. 128, 644–660.
Zhang, Y.-Y., Sun, M., Yuan, C., Long, X.-P., Jiang, Y.-D., Li, P.-F., Huang, Z.-Y., Du, L., 2018. Alternating trench advance and retreat: insights from Paleozoic Magmatism in the Eastern Tianshan, Central Asian Orogenic Belt. Tectonics 37, 2142–2164.
Zhang, X.-R., Chung, S.-L., Lai, Y.-M., Ghani, A.A., Murtadha, S., Lee, H.-Y., Hsu, C.-C., 2019a. A 6000-km-long Neo-Tethyan arc system with coherent magmatic flare-ups and lulls in South Asia. Geology 47, 573–576.
Zhang, X.R., Zhao, G.C., Han, Y.G., Sun, M., 2019b. Differentiating advancing and re-treating subduction zones through regional zircon Hf isotope mapping: a case study from the Eastern Tianshan, NW China. Gondwana Res. 66, 246–254.
Zhao, Z.H., Xiong, X.L., Wang, Q., Wyman, D.A., Bao, Z.W., Bai, Z.H., Qiao, Y.L., 2008. Underplating-related adakites in Xinjiang Tianshan, China. Lithos 102, 374–391.
Zhao, Z.-Y., Zhang, Z.-C., Santosh, M., Huang, H., Cheng, Z.-G., Ye, J.-C., 2015. Early Paleozoic magmatic record from the northern margin of the Tarim Craton: further insights on the evolution of the Central Asian Orogenic Belt. Gondwana Res. 28, 328–347.
Zhong, L.L., Wang, B., Shu, L.S., Liu, H.S., Mu, L.X., Ma, Y.Z., Zhai, Y.Z., 2015. Structural overprints of early Paleozoic arc-related intrusive rocks in the Chinese Central Tianshan: implications for Paleozoic accretionary tectonics in SW Central Asian Orogenic Belts. J. Asian Earth Sci. 113, 194–217.
Zhong, L.-L., Wang, B., Alexeiev, D.V., Cao, Y.-C., Biske, Y.S., Liu, H.-S., Zhai, Y.-Z., Xing, L.-Z., 2017. Paleozoic multi-stage accretionary evolution of the SW Chinese Tianshan: New constraints from plutonic complex in the Nalati Range. Gondwana Research 45, 254–274.
Zhong, L.L., Wang, B., de Jong, K., Zhai, Y.Z., Liu, H.S., 2019. Deformed continental arc sequences in the South Tianshan: new constraints on the Early Paleozoic accretionary tectonics of the Central Asian Orogenic Belt. Tectonophysics 768, 228169.
Zhou, J.-B., Wilde, S.A., 2013. The crustal accretion history and tectonic evolution of the NE China segment of the Central Asian Orogenic Belt. Gondwana Res. 23, 1365–1377.
Zhou, D., Graham, S.A., Chang, E.Z., Wang, B., Hacker, B., 2001. Paleozoic tectonic amalgamation of the Chinese Tian Shan: evidence from a transect along the Dushanzi-Kuqa Highway. In: Hendrix, M.S., Davis, G.A. (Eds.), Paleozoic and Mesozoic Tectonic Evolution of Central Asia: From Continental Assembly to Intracontinental Deformation. Geological Society of America Memoir, Boulder, Colorado, pp. 23–46.
Zhou, J.-B., Wilde, S.A., Zhao, G.-C., Han, J., 2018. Nature and assembly of micro-continental blocks within the Paleo-Asian Ocean. Earth Sci. Rev. 186, 76–93.
Zhu, Y.F., 2011. Zircon U-Pb and muscovite $^{40}Ar/^{39}Ar$ geochronology of the gold-bearing Tianger mylonitized granite, Xinjiang, northwest China: implications for radiometric dating of mylonitized magmatic rocks. Ore Geol. Rev. 40, 108–121.
Zhu, Y., Guo, X., Song, B., Zhang, L., Gu, L., 2009. Petrology, Sr-Nd-Hf isotopic geochemistry and zircon chronology of the Late Palaeozoic volcanic rocks in the southwestern Tianshan Mountains, Xinjiang, NW China. J. Geol. Soc. 166, 1085–1099.
Zhu, D.-C., Zhao, Z.-D., Niu, Y., Mo, X.-X., Chung, S.-L., Hou, Z.-Q., Wang, L.-Q., Wu, F.-Y., 2011. The Lhasa Terrane: record of a microcontinent and its histories of drift and growth. Earth Planet. Sci. Lett. 301, 241–255.
Zhu, D.C., Wang, Q., Zhao, Z.D., Chung, S.L., Cawood, P.A., Niu, Y., Liu, S.A., Wu, F.Y., Mo, X.X., 2015. Magmatic record of India-Asia collision. Sci. Rep. 5, 14289.
Zhu, D.C., Wang, Q., Zhao, Z.D., 2017. Constraining quantitatively the timing and process of continent-continent collision using magmatic record: method and examples. Sci. China Earth Sci. 60, 1040–1056.
Zhu, X., Wang, B., Chen, Y., Liu, H.S., Horng, C.-s., Choulet, F., Faure, M., Shu, L.S., Xue, Z.H., 2018a. First early permian paleomagnetic Pole for the Yili Block and its implications for late Paleozoic postorogenic kinematic evolution of the SW Central Asian Orogenic Belt. Tectonics 37, 1709–1732.
Zhu, X.Y., Wang, B., Cluzel, D., He, Z.Y., Zhou, Y., Zhong, L.L., 2019. Early Neoproterozoic gneissic granitoids in the southern Yili Block (NW China): constraints on microcontinent provenance and assembly in the SW Central Asian Orogenic Belt. Precambrian Res. 325, 111–131.